Eur. Phys. J. A (2018) **54**: 97
DOI 10.1140/epja/i2018-12528-0

THE EUROPEAN PHYSICAL JOURNAL A

Review

The ACCULINNA-2 project: The physics case and technical challenges

A.S. Fomichev[1,2,a], L.V. Grigorenko[1,3,4], S.A. Krupko[1], S.V. Stepantsov[1], and G.M. Ter-Akopian[1,2]

[1] FLNR JINR, 141980 Dubna, Moscow region, Russia
[2] State University DUBNA, 141980 Dubna, Moscow region, Russia
[3] NRC "KI", 123182 Moscow, Russia
[4] NRNU "MEPhI", 115409 Moscow, Russia

Received: 22 February 2018 / Revised: 28 April 2018
Published online: 18 June 2018

Communicated by N. Alamanos

Abstract. Implementing the Dubna Radioactive Ion Beams project (DRIBs) a new, efficient fragment separator ACCULINNA-2 was installed recently at the primary beam line of the U-400M cyclotron in the Flerov Laboratory of Nuclear Reactions, JINR. Since 2017, radioactive beams have been obtained from this facility. The motivation for the new RIB complex, together with an overview of the RIB research conducted in Dubna and its correlation with the worldwide RIB activities, are given in this paper. The status of the ACCULINNA-2 setup, the nearest prospects for completing its equipment, and the planned first-stage experiments are presented.

1 Introduction

One of the main trends in the modern nuclear-physics instrumentation consists in the construction of the so-called radioactive ion beam (RIB) "factories" [1–11] made for the study of the nuclear systems away from the "stability valley". Among the principal goal of such research is the trend to achieve the nuclear driplines and move further beyond the driplines as far as possible. Until recently the only fully working RIB facility in Russia was the fragment separator ACCULINNA in the Flerov Laboratory of Nuclear Reactions (FLNR), JINR. The scientific yield [12] made with this facility (some results of this study are given in sect. 2) inspired the construction of a new fragment separator ACCULINNA-2 [13]. This facility was built in collaboration with SIGMAPHI company, France [14–16]. The separator was installed on the primary beam line of the U-400M cyclotron, see fig. 1. Test runs made in 2017 showed that the characteristics of RIBs delivered by ACCULINNA-2 match perfectly the initial design.

At the current level of funding the up-to-date experimental program at ACCULINNA-2 should concentrate on the research topics where this facility could offer unique opportunities and methods. The choice made is focused on the study of light nuclear systems far from the stability valley. We mean the program of searches for $2n$ and $4n$ radioactivity, as well as the study of the $2n$, $4n$, $2p$, $4p$ decay modes of nuclei near the borders of nuclear stability. These studies will be accomplished with the use of unique cryogenic-target systems, in particular the targets of hydrogen (including tritium) and helium isotopes [14,15]. A key feature of the target complex, together with the modern detector systems (microstrip silicon detectors, gamma array, neutron wall, optical time projection chamber etc.), is the high detection efficiency of the reaction products emitted within the solid angle 2–6 sr in the center of mass system. This provides enhanced capability in revealing specific reaction channels and makes available significant additional information actually needed for the spin-parity identification of newly obtained exotic resonance states.

The advantage of our methodology for the study of neutron-rich (^{7}H, ^{10,12}He, ^{10}Li, ^{16}Be, ^{26}O etc.) and proton-rich (^{6}Be, ^{12}O, ^{17}Ne, ^{26,27}S etc.) nuclei is the use of few-nucleon transfer reactions for the population of their excitation spectra coming about in collisions with the relatively low-energy secondary beams ($\sim$ 20–40 A MeV). This provides significant additional information actually needed for the spin-parity identification. It is noteworthy that there is the lack of such information in the case of knockout (fragmentation) reactions representing the main approach used in the case of higher ($\sim$ 70–500 A MeV) energies available for the other modern RIB facilities.

The realization of these ambitious purposes calls for specific conditions imposed on the created RIB facility and on the employed experimental techniques. Therefore,

[a] e-mail: fomichev@jinr.ru

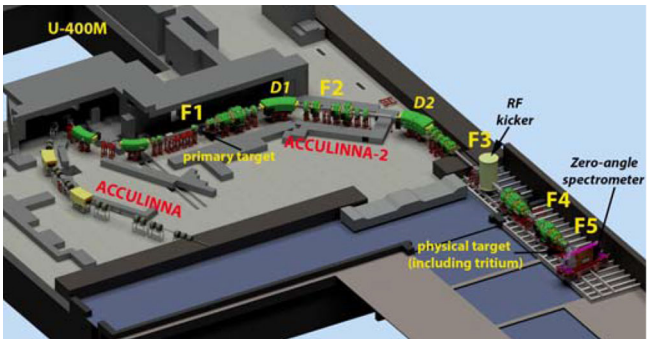

Fig. 1. Layout of the ACCULINNA and ACCULINNA-2 fragment separators at U-400M cyclotron.

the prime objectives of ACCULINNA-2 are to provide a good energy resolution for the beams of radioactive nuclei and high efficiency for correlation measurements. ACCULINNA-2 is proposed to become a versatile instrument with a broad range of methods allowing one to extract the searched information in experiments assuming the study of different reactions: elastic and inelastic scattering, resonant scattering, transfer reactions, Coulomb dissociation, breakup reactions in general and the spectroscopy in a continuum, knockout reactions and quasifree scattering, radioactive decays, fusion-evaporation and incomplete fusion reactions.

This paper is intended to give a view about the field of research assumed by the authors for the RIB separator ACCULINNA-2 commissioned recently in FLNR. The summary of the main subjects and studies foreseen at the facility and the general information on the separator are given in sect. 1, Introduction. Section 2 is destined to give the notion to the reader on the transfer-reaction studies made since 1996 with the RIBs provided by the ACCULINNA separator. The knowledge acquired about the ground-state structures and resonance spectra of light drip-line nuclei is summarized here, along with the prospective approaches, made to examine the resonant states in drip-line nuclei. Section 3 gives specific information about the design of the ACCULINNA-2 separator, its ion-optical parameters and technical solutions implemented in order to produce a variety of intense RIBs. The research program anticipated for this facility is the subject discussed in sect. 4. The performance capacity achieved with ACCULINNA-2 allowed to begin in 2017 and to carry out the first experiments foreseen in the designed research program. These topics are outlined in sect. 5, and the studies foreseen for the realization within the coming seven-year period are discussed in sect. 6. Finally, sect. 7 is given for summary and acknowledgements.

2 Towards ACCULINNA-2

Fragment separator ACCULINNA[1] is working since 1996. Initially, it was intended as an injector for the K4/K10 acceleration-storage ring complex [17]. The setup was built out of magnets that were at hand from spare set of the U-400M cyclotron [18] and adapted mainly for primary beam lines. In 2000 the separator was significantly upgraded, namely it was extended into the neighboring low-background room and equipped with a modern reaction chamber housing cryogenic targets including tritium; acceptance was increased by about 30 percent because of several more powerful quadruples and their rhombic-form tubes [19]. Since that time a series of precision experiments aimed at the study of the lightest neutron rich isotopes ^{4,5,7}H, $^{6-10}$He and proton rich nuclei ^{6}Be, ^{17}Ne, ^{26}S has been performed.

The ACCULINNA group has proposed, developed and practically applied a novel approach to the investigation of resonant states in the spectra of nuclei near and beyond the driplines. We did not restrict the study of resonant states to the derivation of invariant or missing mass spectra. We were able to show that, in experiments performed with certain kinematical setting, correlations inherent to the reaction products become an extremely rich source of information. Another, unique technical feature of the ACCULINNA setup is the availability of intensive tritium beam and cryogenic tritium targets (in gaseous and liquid phases). In this way, the following significant results were obtained at ACCULINNA.

The dineutron and $t+t$ configurations in the structure of the neutron-halo ^{6}He nucleus were experimentally established as a result of measurements done in wide angular ranges for the elastic $^{6}\mathrm{He}+{}^{4}\mathrm{He}$, $^{6}\mathrm{He}+p$ scattering and the $^{6}\mathrm{He}+p\to\alpha+t$ reaction cross-sections [20–23]. The cluster structure of ^{6}He was studied also in quasi-free scattering reaction $^{6}\mathrm{He}+{}^{4}\mathrm{He}\to\alpha+\alpha+2n$ [24]. Detecting here the two α particles outgoing from the target one finds out the missing mass of the $2n$ spectator.

For the first time the spectra of the $^{3}\mathrm{H}(^{2}\mathrm{H},p)^{4}\mathrm{H}$ and $^{3}\mathrm{H}(^{3}\mathrm{H},d)^{4}\mathrm{H}$ reaction products, arising from the population of the ^{4}H ground state resonance, were disentangled from events coming from different reaction mechanisms and the parameters of the ^{4}H ground state were reliably derived [25].

The ^{5}H spectrum has been reliably established. This result was achieved in a series of works [26–30], in active polemics with the results coming from the other groups. Experimental methods for the analysis of the three-body decays of spin-aligned states were developed and successfully applied in practice [29,30]. In the case of ^{7}H a lower limit for its decay energy was established [31].

Low energy spectra of the ^{8}He, ^{9}He and ^{10}He isotopes were significantly revised in [32–37]. Before these works, the low-lying spectra of these nuclei have been considered as reliably established for more than a decade.

Accurate data on the three-body $\alpha+p+p$ continuum of ^{6}Be system were obtained in the charge-exchange $p(^{6}\mathrm{Li},{}^{6}\mathrm{Be})n$ reaction. In the whole range of excitation energy up to 16 MeV the ^{6}Be spectrum was well described by assuming the population of 0^{+} state at 1.37 MeV, 2^{+} state at 3.05 MeV and a mixture of negative parity continuum $(0^{-},1^{-},2^{-})$ in the range from 4 to 16 MeV [38]. It could

[1] The name represents an old Russian women name.

be interpreted as a novel phenomenon – manifestation of the isovector soft dipole mode.

More details about distinctive features appearing at the democratic decay of different nuclear systems (*e.g.* ^{6}Be, ^{12}O, ^{16}Ne, ^{5}H, ^{10}He, ^{26}O), having different ground-state widths, were reported in the review [39]. It is important to note that the width approaching a value of $\Gamma \sim 1\,\mathrm{MeV}$ defines the boundary between the nuclear structure and the dynamics being typical for the continuum spectrum. As a result, the observed spectrum becomes dependent on the population conditions and reaction mechanism. A precise analysis of such dependence was demonstrated by the examples of ^{5}H [32–34], ^{10}He [36,37], ^{6}Be [40], and ^{26}O [41].

The unknown isotope ^{26}S, expected to decay by two-proton ($2p$) emission, was studied theoretically and was searched experimentally among the fragmentation products of beam nuclei ^{32}S bombarding the beryllium production target of the ACCULINNA separator [42]. Based on the obtained production systematics, an upper limit of $T_{1/2} < 79\,\mathrm{ns}$ was established for the half-life time ^{26}S from the known time of flight (TOF) of its nuclei through the fragment separator. Together with the theoretical lifetime estimates made for the two-proton decay, this gives a decay-energy limit of $Q_{2p} > 640\,\mathrm{keV}$ for ^{26}S. In the case that the one-proton emission is the main branch of the ^{26}S decay, a limit $Q_{2p} > 230\,\mathrm{keV}$ would follow for this nucleus.

The experimental determination of the partial width for the first excited state of ^{17}Ne (1288 keV, $3/2^{-}$) with respect to the $2p$ decay mode is another goal being important for the development of the "true" $2p$-decay theory and for clarifying the role of the three-body radiative capture reaction $^{15}\mathrm{O} + 2p$ as a bypass for the ^{15}O waiting point of the astrophysical rp-process [43]. A new approach, based on the combined use of the missing mass and invariant mass methods, has been suggested, developed and successfully tested in experiments carried out recently [46,47].

With the use of the modern Optical Time-Projection Chamber (OTPC), which was first tested with the RIB at ACCULINNA [48], rare beta-decay channels of ^{8}He into the $\alpha + t + n$, $^{6}\mathrm{He} + d$ and $^{7}\mathrm{Li} + n$ [49] and of ^{6}He into the $\alpha + d$ [50] were investigated.

Thus, having a modest technical base and low expenses, the ACCULINNA separator delivers important novel results. How the success of this project could be developed? First of all, it is necessary to outline what was the source of the interesting physics results obtained at this facility. The following factors should be emphasized:

1) The record intensity of the primary cyclotron beams (*e.g.*, 3–5 pμA of ^{11}B).
2) Relatively low (compared to the other in-flight separators) beam energy. This provides a prerequisite for quite a good energy resolution in the measurements done in different experimental conditions. Sufficiently high reaction cross sections corresponding to the RIB energies accessible at ACCULINNA partly compensate for the low intensities of secondary beams.
3) The energy range of exotic beams provided by ACCULINNA is optimal for the nuclear structure studies done by means of transfer reactions. Due to the transparent reaction mechanism this class of reactions is well understood and clear explanation becomes available for the data obtained in such experiments.
4) Complete kinematical measurements are performed routinely. As a result, very clean, background-free spectra are obtained.
5) The essential consequence of such correlation measurements is the possibility of unambiguous spin-parity identification for the observed resonance states. The choice of kinematical conditions selecting specific reaction mechanisms (*i.e.*, direct transfers, quasi-free scattering, spin alignment in zero geometry transfers) simplifies the data interpretation.

2.1 Need for further developments

Over the last few years of ACCULINNA operation, the need for further development of the in-flight RIB separation technique based on the primary beams delivered by the U-400M cyclotron has become obvious.

1) The existing separator with the one-stage RIB cleaning is efficient only for the lightest neutron rich nuclei. It does not cope with the request of high intensity clean beams of very neutron rich and very proton rich nuclei with atomic numbers $Z > 8$. *E.g.*, for the proton-rich nuclei, the contamination level in the secondary beam is too high for efficient operation.
2) The large emittance of the secondary beams obtained from the relatively low-energy primary beams provided by the U-400M cyclotron conflicts with the small acceptance of the existing separator. This leads to severe limitations in the intensity of the most exotic beams. Such RIBs of prime interest as ^{11}Li, ^{14}Be, ^{17}B, ^{19}B, ^{9}C, ^{13}O, ^{17}Ne, etc. are available now only with very low intensities.
3) More powerful detector arrays are required for efficient measurements of multiple-coincidence events. The existing experimental area becomes too small to hold all the needed equipment. This imposes restrictions on the instrumentation positioned upstream (*e.g.*, extra focusing elements) and downstream of the reaction chamber installed at ACCULINNA near its final focal plane (*e.g.*, wide aperture arrays for neutron TOF measurements, the set-ups for detecting reaction products outgoing close to zero angle, etc.).
4) The small length of the separator imposed major limitations on the energy resolution in many experiments: the final resolution is largely defined by the resolution attainable in the measurement of the incoming beam energy. The energy resolution is now limited mainly by the short TOF base attainable at ACCULINNA.

Evidently the next-generation facility should enhance the advantageous features of the existing facility and eliminate/diminish the disadvantages as much as possible. The next-generation fragment separator is expected to be a

Table 1. Characteristics of several in-flight RIB separators. Abbreviations mean: $\Delta\Omega$: angular acceptance, δ_P: momentum acceptance, $P/\Delta P$: the first-order momentum resolution estimated taking a 1 mm object size. Since 2020 (after U-400M modernization) intensities of ions with $Z \leq 36$ at ACCULINNA-2 will be comparable with RIPS, RIKEN [10].

		ACC	ACC-2	LISE3	ARIS[a]	RIPS	BigRIPS[a]	FRS	SuperFRS[a]
		FLNR, JINR		GANIL	FRIB	RIKEN		GSI/FAIR	
$\Delta\Omega$	msr	0.9	4.2	1.0	5.0	5.0	6.3	0.32	5.0
δ_P	%	2.5	6.0	5.0	10	6.0	6.0	2.0	5.0
$P/\Delta P$	a.u.	1000	2000	2200	4000	1500	3300	8600	3050
$B\rho_{max}$	Tm	3.2	3.9	3.2-4.3	8.0	5.76	9.0	18	18
Length	m	21	37	19(42)	87	21	77	74	140
$E_{\min}$	AMeV	10	5	30	30[b]	30	5[c]	220	
$E_{\max}$	AMeV	40	50	80	300	90	350	1000	1500

[a] Super-conducting magnets are used in the ion-optical system.
[b] Low-energy domain below 30 A MeV is also possible.
[c] In the frame of OEDO (Optimized Energy Degrading Optics for RIB) project, `http://www.cns.s.u-tokyo.ac.jp/oedo/wiki/`.

more universal and powerful instrument. The beam intensities should be increased, the beam quality improved, and the range of the accessible secondary radioactive beams should be extended.

2.2 Scientific diversification

The fragment separator ACCULINNA was able to furnish exceptional conditions for progress in the studies of light exotic nuclei [39]. On the other hand, some diversification of the research program carried out at this facility is needed. In the long-time prospect it is not acceptable that the whole research at the facility is only focused on the reactions involving several nuclei. It does not mean that the reaction studies with heavier neutron-rich and even with certain proton-rich RIBs are not possible at ACCULINNA, but such experiments would suffer from considerable difficulties hindering the above mentioned advantages of the ACCULINNA facility and impeding the advance towards the up-to-date, high-class scientific results. The proposed development of the ACCULINNA-2 fragment separator offers the creation of a more universal scientific instrument giving a variety of clean and well-prepared secondary beams limited only by the choice of the primary beams provided by the U-400M cyclotron.

An important task of the ACCULINNA-2 project is the realization of the beam usage concept at FLNR complying with the modern trends inherent to the large RIB facilities. The fragment separator, together with the beam diagnostics system, should become a *standard instrument* for the laboratory. The idea is that the exotic beam is delivered for the users into the low-background experimental area with full particle-by-particle identification and additional diagnostics (energy/angle). Nowadays, such an approach is standard at the large international RIB facilities. The ultimate purpose is that the secondary beam users should not worry about the incoming beam at all. This facilitates the RIB use by different groups carrying out various experiments.

The development of new detector systems and mastering modern digital technologies for the ACCULINNA-2 project include:

1) Zero-angle magnetic spectrometer providing conditions needed for the detection of beam-like reaction products in the case of the high RIB intensity [14,39].
2) New generation of micro-strip silicon detectors dedicated to tracking/spectroscopy experiments [51].
3) Radiation-hard and extremely fast silicon detectors providing a very good time resolution ($\sigma \sim 50$ ps) for TOF measurements and beam diagnostics [52].
4) Neutron detector arrays based on stilbene crystals [53], scintillation fibers and conventional multi-layer plastic scintillator arrays [51].
5) Arrays of CsI, $LaBr_3$, etc. crystals for the charged-particle and gamma-ray detection [51].
6) Substantially upgraded OTPC operating at $P \sim 0.5$–3.0 Atm. One should significantly improve the quality of observed trajectories of charged particles and the precision of 3D-coordinate measurements.
7) Universal data acquisition system (like MBS - Multi Branch System or compatible one) capable of combining the main standards of digital electronics modules (VME, VXI, Fastbus, CAMAC), see ref. [54].

2.3 Scientific uniqueness and anticipated agenda

ACCULINNA-2 separator is not intended to compete with the new large in-flight RIB separator devices (SuperFRS at FAIR [7,8], ARIS at FRIB [9], BigRIPS at RIKEN [11] or others [3–6], see table 1 and fig. 2) in the sense of "crude power". It should complement the existing/constructed facilities in certain fields. Namely, ACCULINNA-2 should provide high intensity RIBs in the lowest energy range attainable for the in-flight separators. We emphasize the scientific importance of the corresponding field of research and consequently we choose a cost-effective technical solution for this project. Within a minor fraction of the total

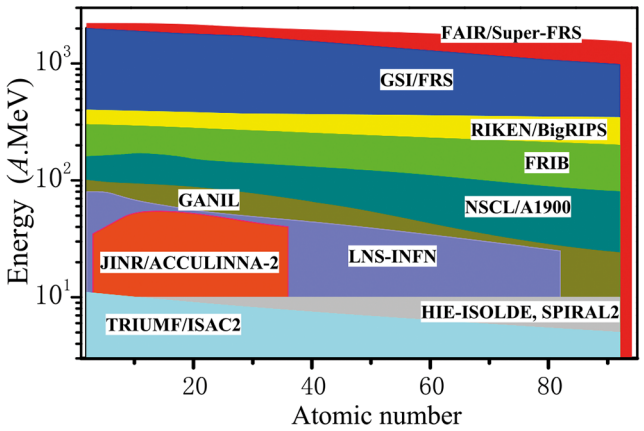

Fig. 2. Landscape of the present-day facilities on the diagram where for radioactive beams, specified in terms of their atomic numbers, the available RIB energy ranges are shown.

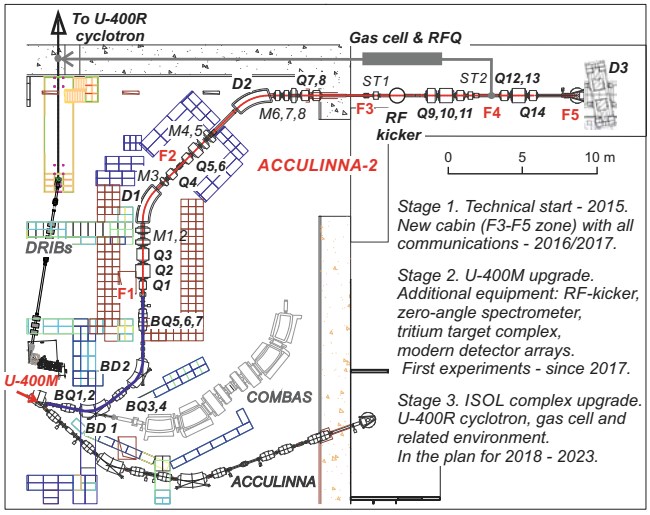

Fig. 3. Scheme of the ACCULINNA-2 fragment separator in the U-400M cyclotron hall. Indicated on the right side is the list of scheduled developments.

cost of the modern RIB facilities[2] it is possible to pursue world-class research due to a *specific scientific focus* of this instrument. The prime objectives of ACCULINNA-2 are to provide *a good energy resolution* for the beams of radioactive nuclei and high efficiency for *correlation measurements*. The latter, combined with the selection of certain reaction mechanisms and the choice of specific kinematical conditions, could provide the spin-parity identification made for the excitation spectra of the studied exotic nuclei. In that case, the relatively low-energy secondary beams will provide a unique position for ACCULINNA-2 between the other fragment separators. So far, the energies in a range of 10–40 A MeV are not so easily available at other large-scale in-flight RIB separators.

The availability of such beams clears the way towards the implementation of research works in a number of contemporary basic fields in nuclear physics. The investigation of nuclei far from β-stability valley and even beyond the nuclear stability lines is important for understanding the properties of nuclear matter at the extreme conditions. It is also necessary for the further development of nuclear theory and indispensable for nuclear astrophysics.

The proposed ACCULINNA-2 project is focused on the study of nuclear properties far from the stability valley. Near the proton or neutron drip-lines, the emission thresholds of nuclear systems of a few nucleons (clusters) become close to the ground state (evidently, beyond the drip-lines these thresholds are below the ground state). Close to the thresholds, the clusterization phenomenon becomes increasingly important: some nuclear states possess expressed cluster structures, and new forms of nuclear dynamics arise. Among these, the following should be mentioned: i) nucleon haloes (neutron skins, Efimov states, etc.); ii) soft excitation modes (*e.g.*, the soft mode of the giant dipole resonance); iii) new magic numbers and intruder states; iv) $2p$, $4p$, $2n$ and $4n$ radioactive decays (few body decays in general terms).

[2] Amount paid for the ACCULINNA-2 project made $\sim$ 7 M$.

The research focused on nuclear astrophysics and novel forms of nuclear dynamics presumes a dedicated scientific program, high intensity beams, and specialized instrumentation suitable for carrying out precision measurements. Two ways are possible to overview the scientific agenda. Looking from the side of physical problems we single out the topics of nuclear reactions, nuclear structure, and nuclear astrophysics as the main broad-scope challenges for the scientific agenda of ACCULINNA-2. Each of these major research directions has a preferable set of methods by which its problems could be best handled. Therefore, another way to look at the scientific agenda of the ACCULINNA-2 separator is to consider *optimal physical methods* to study the properties of those nuclear systems which should be accessible with this instrument. It is clear that similar experimental methods can be used to settle different physical matters with smaller or larger success.

3 Technical challenges of the new facility

To meet the conditions requested by the proposed scientific program the following technical features of the fragment separator ACCULINNA-2 are foreseen.

The schematic layout of ACCULINNA-2 placed within the U-400M cyclotron hall is shown in fig. 3. A beam of radioactive nuclei leaving the production target at the F1 focal plane is captured by a short-focusing quadrupole triplet $Q1$-$Q3$ and is transported through the magnetic dipoles $D1$-$D2$ and magnetic quadrupoles $Q4$-$Q14$ up to the final focal plane F5. The F2 non-zero momentum dispersion plane is intended for the installation of a wedge-shaped energy degrader. In the achromatic focal plane F3 the separation of the secondary beams with mass A and charge Z takes place (bare nuclei are implied) according to the cumulative effect of the $\%B\rho$ separation in the F2 plane and the charge-mass dependence of the ΔE energy losses in the wedge. For the neutron-excess fragmentation

Table 2. Ion-optical parameters of the RF kicker system.

Electrode vertical gap	$2h$	cm	7
Electrode width	$2w$	cm	12
Electrode length	L	cm	70
Cylinder diameter	D	cm	120
Length of coaxial line	H	cm	183
Electric field amplitude	$E_{\max}$	kV/cm	15
Frequency range	f	MHz	15–22

Table 3. Main ion-optical parameters of ACCULINNA-2.

Primary beam spot size	F1	2×2	mm^2
Momentum acceptance		6.0	%
θ_{0x} angular acceptance		60	mrad
θ_{0y} angular acceptance		70	mrad
X momentum dispersion	F1 $\rightarrow$ F2	2.0	cm/%$B\rho$
θ_x angul. mom. disper.	–	0.5	mrad/%$B\rho$
X magnification	–	-1.0	
Y magnification	–	-7.4	
X momentum dispersion	F2 $\rightarrow$ F3	3.3	cm/%$B\rho$
X magnification	–	-1.7	
Y magnification	–	-2.0	
X magnification	F1 $\rightarrow$ F3	1.7	
Y magnification	–	5.0	
Length	F1 $\rightarrow$ F2	9.51	m
Length	F2 $\rightarrow$ F3	14.35	m
Length	F3 $\rightarrow$ F4	7.63	m
Length	F3 $\rightarrow$ F5	13.25	m
Length	F1 $\rightarrow$ F5	37.1	m

products this separation is typically enough for preparing quite pure beams.

Proton-rich radioactive beams suffer from a large amount of contaminations. To cope with this problem, a vertically deflecting radio-frequency (RF) kicker [55] is foreseen to be installed just after the achromatic focal plane F3 between the steering magnet $ST1$ and quadrupole $Q9$. The RF transverse electric field causes a phase-dependent transverse deflection of ions. The technical parameters of the RF kicker are presented in table 2. The two steering magnets $ST1$ and $ST2$ compensate at the position of the F4 slit the vertical shift of the centroid of the beam of interest when the beam passes the RF kicker on the crest of the RF wave. The majority of the unwanted ions come to the F4 plane being beyond the vertical slit. The RF kicker is planned to be installed in 2018.

The most important second-order aberrations in the F2 and F3 focal planes are corrected by the magnetic sextupoles lenses $M1$, $M3$, $M4$, $M6$, $M7$. As a result, the (x/θ_{0x}^2), $(x/\theta_{0x}\delta_P)$, and (x/θ_{0y}^2) second-order aberration coefficients, given in the TRANSPORT [56] code

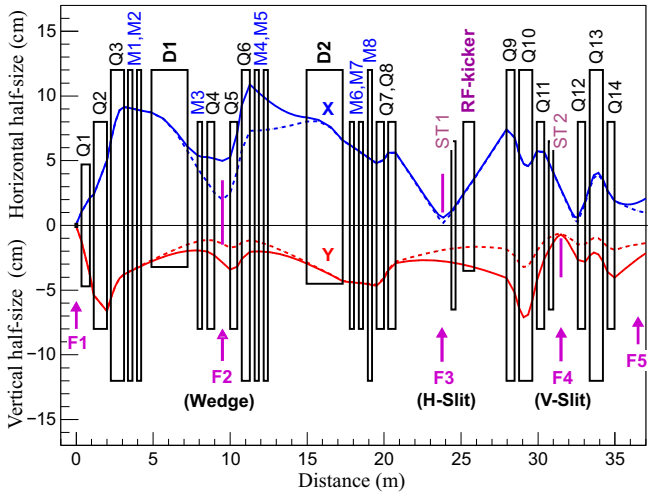

Fig. 4. Envelopes of the beam in horizontal (X) and vertical (Y) planes. F1 object slit is 2×2 mm^2, capture angles are ± 30 and ± 35 mrad in X and Y planes, respectively. Solid lines are for $\delta_P = \pm 2.5\%$ and dashed ones for $\delta_P = \pm 1.0\%$.

notations, become very small in the F2 and F3 planes. A smooth adjustment of the focusing effect in these planes is foreseen by tuning the strengths of the magnetic octupoles lenses $M2$, $M5$, $M8$. A comparison of the new ACCULINNA-2 setup with the other fragment separators is provided in table 1. The main ion-optical parameters of ACCULINNA-2 are listed in table 3. The individual characteristics of the magnetic elements are given in tables 4–6.

The second-order accuracy envelopes for the ion optics, when there are no energy degrading matter elements along the facility layout, are shown in fig. 4. The TRANSPORT code was used for the calculations. There were assumed a 2×2 mm^2 object slit in F1 and that ions were captured by the ion optical system of ACCULINNA-2 within an angular range of ± 30 mrad and ± 35 mrad in the horizontal and vertical directions, respectively, and momentum spread of $\pm 2.5\%$. The chosen beam spot is optimised for the thermal load of production targets and angular divergence of primary beams. Some trajectories calculated with GICOSY [57] code are shown in fig. 5. The first-order cosine- and sine-like functions and the horizontal momentum dispersion are given in fig. 6. The choice of such a layout of the ACCULINNA-2 provides a reasonable compromise between the separation efficiency ($B\rho_{\max}$ plus acceptances) and the facility cost (the goal was to install the setup inside the cyclotron building with the existing infrastructure).

Refined third-order ray-tracing calculations were carried out using the transport matrices generated with GICOSY. The transverse phase space angular acceptances ($\Delta\theta_X$, $\Delta\theta_Y$) as well as the $\delta_P = \Delta P/P$ momentum acceptance calculated for ions passing from F1 to F5 are presented in fig. 7. The calculations were done for a 2×2 mm^2 object slit in F1 plane assuming that the ions escaped from it homogeneously and isotropically in space and uniformly distributed with respect to the momentum. The

Table 4. Ion-optical parameters of ACCULINNA-2 magnetic dipoles $D1$, $D2$ and steering (correcting) magnets $ST1$, $ST2$.

Value		Units	$D1$	$D2$	$ST1$, $ST2$
Bending direction			horizontal	horizontal	vertical
Type			sector	sector	rectangular
Gap height	$2h$	cm	6.4	9.0	11.2
Bending mean radius	R	m	3.0	3.0	–
Bending field	$B_{\rm nom}$	T	1.3	1.3	0.053
Length	$L_{\rm eff}$	m	2.356	2.356	0.283
Working width	$2w$	cm	20	20	10
Bending angle	Φ	dgr	45	45	–
Entrance angle	$\tau_{\rm entr}$	dgr	0	0	0
Exit angle	$\tau_{\rm exit}$	dgr	0	20	0

Table 5. Ion-optical parameters of ACCULINNA-2 magnetic quadrupoles.

Value		units	$Q1$	$Q2$	$Q3$, 10, 13	$Q4$, 5, 7, 8, 11, 12, 14	$Q6$, 9
Aperture	$2r$	cm	9.4	16	24	16	24
Length	$L_{\rm eff}$	cm	54.3	87.1	85.9	47.6	51.8
Field gradient	$G_{\rm nom}$	T/m	9.2	7.2	7.2	9.8	6.4

Table 6. Ion-optical parameters of magnetic multipoles. They all have an effective length $L_{\rm eff} = 28.6$ cm.

Multipole	Aperture $2r$, cm	Sextupole $B''_{\rm nom}$, T/m^2	Octupole $B'''_{\rm nom}$, T/m^3
$M1$, $M2$, $M4$, $M5$, $M8$	24	3.9	195
$M3$, $M6$, $M7$	16	39	

corresponding transverse images in F2 and F3-F5 planes are shown in fig. 8 and fig. 9, respectively.

At real experimental conditions the calculations must be carried out with keeping in mind a type of reaction for RIB production, the transverse and longitudinal acceptances of the facility. The reaction fragments, each of which has at the exit from the production target peculiar energy and angular distributions, are transported to the F5-plane position with taking into account the atomic interaction of these fragments with the target and wedge atoms. As an example, the ^{12}Be RIB was produced by fragmentation of the 49.7 A MeV primary ^{15}N beam on a 2 mm thick Be-target with a diameter of 7 mm. It was purified in a 1 mm thick achromatic Be-wedge for $\delta_P = \pm 2.0\%$. The ^{12}Be beam sizes calculated in the planes F3-F5 are shown in fig. 10. The calculations were performed with the MOCADI [58] code.

These calculations were confirmed well enough during the several beam tests made in 2017, see sect. 5 for more details.

The purification effectiveness of the RF kicker which could be very significant for neutron-deficient beams [55, 59] is demonstrated in fig. 11 in case of ^{28}S. A 32 A MeV ^{28}S beam is produced by the fragmentation of 52 A MeV ^{32}S primary beam on a 92.4 mg/cm^2 Be production target. The achromatic 92.4 mg/cm^2 Be wedge was used in the calculations. After passing the 2 cm width horizontal slit in F3 most of the contaminants are eliminated. The remaining ones are ^{27}P, ^{26}Si, ^{25}Al, and ^{21}Ne. The further purification of the ^{28}S beam is performed with the RF kicker. At a frequency of 17.9 MHz and an electric field of 15 kV/cm on the crest of the RF-wave the ions in the beam are dispersed along the vertical direction at F4 as shown in fig. 11. By appropriately choosing the width and position of the vertical slit at F4, it is possible to purify the beam of ^{28}S up to several percents of ^{27}P contamination.

The development of the ACCULINNA-2 facility includes the upgrade of the U-400M cyclotron to produce ^{48}Ca, ^{58,64}Ni and ^{84}Kr primary beams with energies 36–47 A MeV and intensities approaching 1.0 pμA. The 1–3 pμA beams of ^{40}Ca, ^{40}Ar, and ^{36}S with energy 40–45 A MeV will also be available. The cyclotron upgrade includes: i) the installation of a new cryogenic ECR ion source giving $\sim 30\,\mu$A beams of ^{58}Ni^{16+}, ^{48}Ca^{14+} ions and $\sim 10\,\mu$A beam of ^{84}Kr^{20+} ions for injection into the cyclotron; ii) the beam extraction system of the cyclotron will be improved for the whole variety of the possible 30–60 A MeV beams; iii) the necessary shielding should be provided for the primary beam line and for the compartment of the ACCULINNA-2 production target to work with the intense beams of such ions as ^{7}Li, ^{10,11}B, ^{14,15}N, ^{20,22}Ne, etc. At the moment the primary beam intensi-

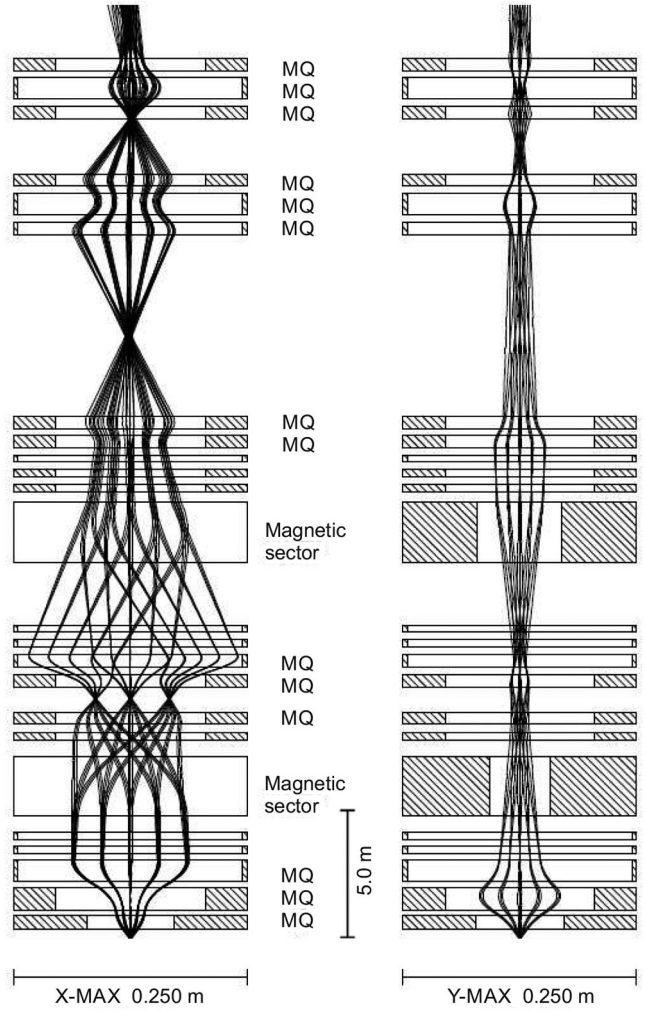

Fig. 5. Some third-order beam trajectories in X (left) and Y (right) planes calculated via GICOSY for $\delta_P = \pm 2.0\%$, $\theta_{0x} = \theta_{0y} = \pm 20$ mrad and an object of $2 \times 2\,\mathrm{mm}^2$.

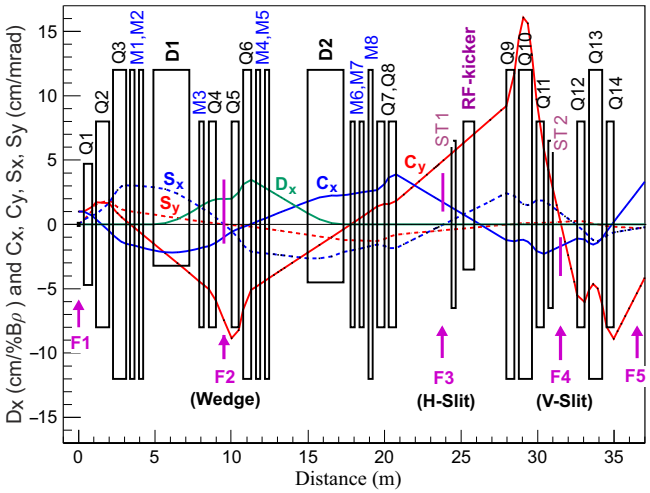

Fig. 6. Momentum dispersion $D_x = (x/\delta_P)$ and main first-order cosine-like, $C_x = (x/x_0)$, $C_y = (y/y_0)$ and sine-like $S_x = (x/\theta_{0x})$, $S_y = (y/\theta_{0y})$ trajectories.

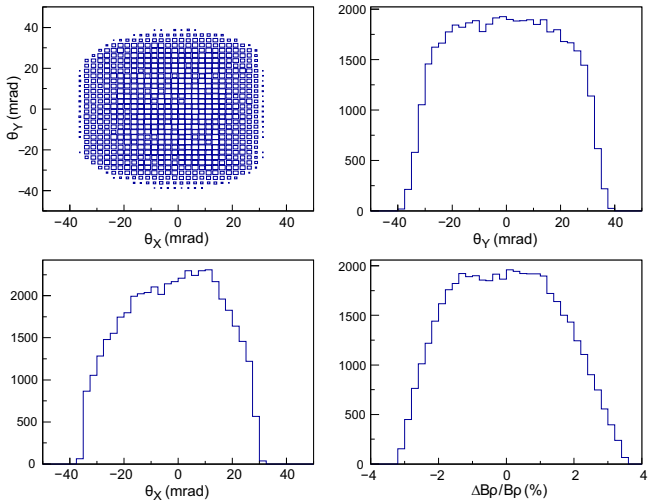

Fig. 7. Overall angular and momentum acceptances of ACCULINNA-2 for an object slit of $2 \times 2\,\mathrm{mm}^2$.

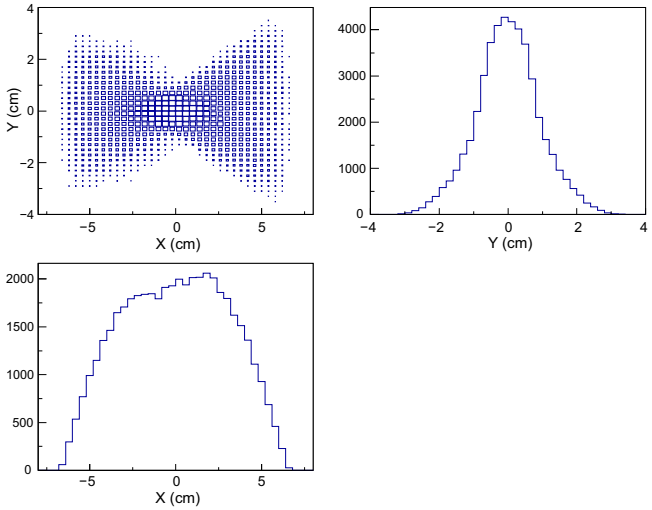

Fig. 8. Spatial distribution of the beam in the dispersive focal plane F2. Object slit is $2 \times 2\,\mathrm{mm}^2$.

ties exceeding $\sim 4\,\mathrm{p}\mu\mathrm{A}$ lead to problems with radiation security.

The RIB generation in the energy range 5–50 A MeV will be provided by ACCULINNA-2 working with the primary beams of the upgraded U-400M. The lower part of this range is suitable for the study based on the use of resonance scattering reactions on a thick target, the intermediate region is optimal to carry out transfer reactions, and the upper part is reasonable for the Coulomb dissociation studies.

RIB quality improvement at ACCULINNA-2 is expected to be the case because of the following circumstances: i) introduction of the sextupole and octupole magnetic elements results in a good momentum resolution in the dispersive (wedge) plane F2 and allows one to focus a large-emittance secondary beam into a ~ 3 cm spot in the F5 plane (see sect. 5); ii) beam quality increases due to the magnetic achromat being supplemented

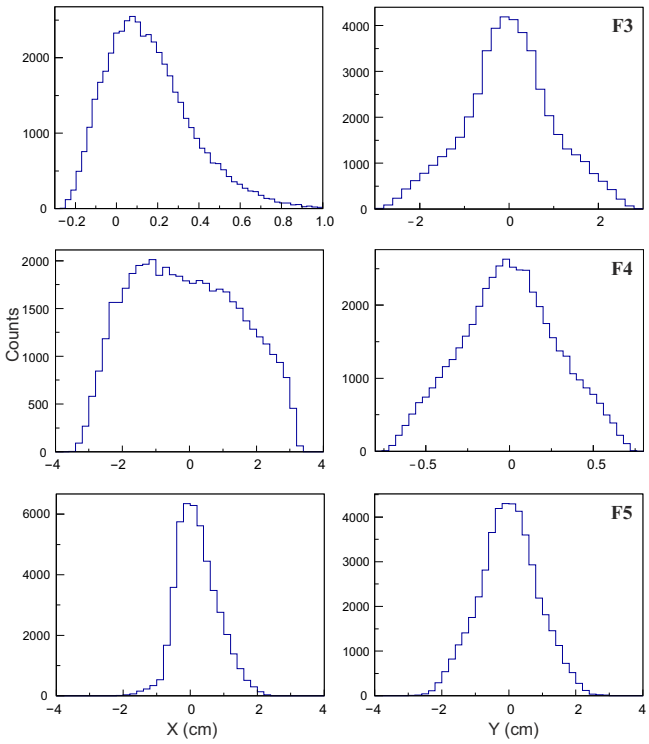

Fig. 9. Transverse images in the F3 (top), F4 (middle) and F5 (bottom) planes. Object slit is $2 \times 2\,\mathrm{mm}^2$.

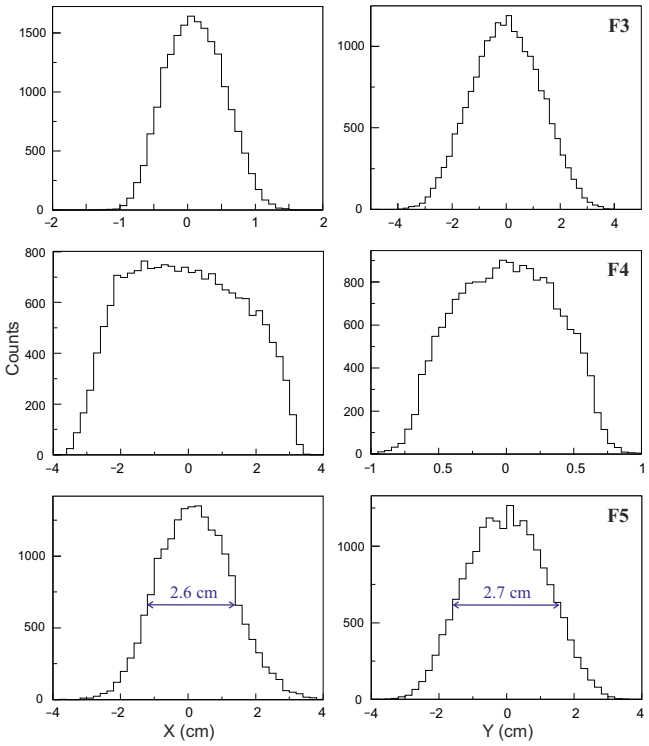

Fig. 10. Calculated beam sizes of ^{12}Be radioactive beam in the F3 (top), F4 (middle) and F5 (bottom) planes, produced at fragmentation of a ^{15}N (49.7 A MeV) primary beam on a Be-target 2 mm thick. Object slit F1 was 7 mm in diameter. Achromatic 1 mm Be-wedge was proposed, $\delta_P = \pm 2.0\%$.

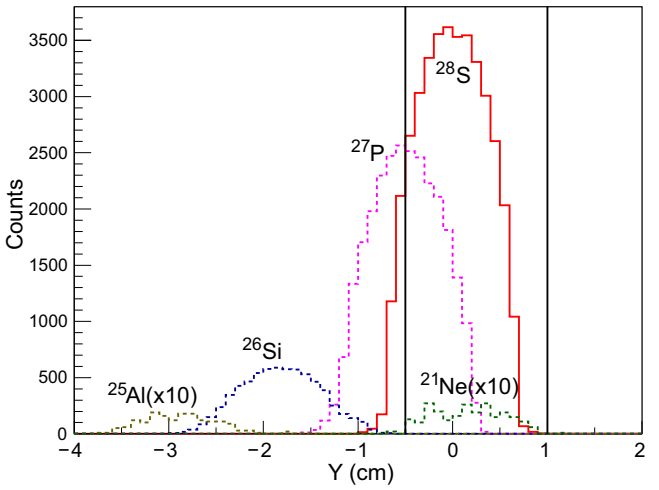

Fig. 11. Relative distribution of transmissions calculated for different isotopes in the vertical direction at the F4-plane as a result of RF purification of the 32 A MeV ^{28}S neutron-deficient beam. Two thick vertical lines show the borders of the slit installed in the F4 plane for blocking the passage of unwanted nuclei.

with the second beam-cleaning stage, namely with the RF kicker. This RF filter with maximal electric field amplitude of 15 kV/cm and frequency in a range of 15–22 MHz allows one to purify well proton-excess RIBs with velocities of up to $\beta = 0.32$ (beam energies up to 50 A MeV); iii) the energy resolution achievable with the TOF measurement made for the secondary ion beam hitting the reaction target should be better than 0.25%. The ion-optical system of ACCULINNA-2 has a TOF base of 13.3 m (the distance between F3 and F5 planes, see fig. 3 and table 3). This is about two times larger than ACCULINNA provides now. Modern TOF start/stop detectors (*e.g.*, diamond or silicon planar micro-strip detectors) should improve the time resolution (FWHM) from 400 ps, routinely achieved now, to a level of better than 50 ps.

The primary beams supplied by the U-400M cyclotron at present time, when ACCULINNA-2 is put into operation, are specified in table 7. After the cyclotron upgrade made in 2019 the beam intensities presented in this table will increase by 2–3 times, and their energy will rise by $\sim$ 12 percents. As a result the following beam properties are expected from the ACCULINNA-2 separator.

i) The range of delivered RIBs will be broaden considerably. The $E = 36\,A$ MeV primary ^{86}Kr^{24+} beam can be produced by the U-400M cyclotron being supplied at present with a new superconducting ECR ion source. Thus, RIBs with atomic numbers up to $Z = 36$ are expected to be produced and separated at ACCULINNA-2.

ii) The estimated intensities of the proton-rich beams (*e.g.* ^{8}B, ^{9}C, ^{13}O, ^{14}O, ^{17}Ne, ^{20}Mg, etc.) and of neutron-rich beams (*e.g.* ^{11}Li, ^{12}Be, ^{14}Be, ^{15}B, ^{17}B, etc.) are found in a range of 3×10^4–$3 \times 10^5\,\mathrm{s}^{-1}$.

iii) Contamination level in the beams of ^{6}He, ^{8}He, ^{9}Li, ^{11}Be, ^{12}Be is expected to be no more than 2–10% and in the beams of ^{8}Be, ^{9}C, ^{11}Li, ^{13}O, ^{14}Be, ^{14}O, ^{15}B, ^{17}B,

Table 7. U-400M cyclotron beams available for delivery to the ACCULINNA-2 fragment separator. The beam energies indicated in the third column will raise by $\sim$ 12% after the upgrade of the U-400M cyclotron, planned for 2019.

Beam	Energy, A MeV	Intensity, pμA (pps)
$^{7}Li^{2+}$	34	5 (3.1×10^{13})
$^{10}B^{3+}$	39	3 (1.9×10^{13})
$^{11}B^{3+}$	32	3 (1.9×10^{13})
$^{12}C^{4+}$	48	3 (1.9×10^{13})
$^{13}C^{4+}$	41	3 (1.9×10^{13})
$^{15}N^{5+}$	49	2 (1.3×10^{13})
$^{16}O^{5+}$	42	2 (1.3×10^{13})
$^{18}O^{5+}$	33	1 (6.3×10^{12})
$^{18}O^{6+}$	54	1[a] (6.3×10^{12})
$^{20}Ne^{7+}$	53	1 (6.3×10^{12})
$^{22}Ne^{7+}$	44	1 (6.3×10^{12})
$^{32}S^{11+}$	52	1 (6.3×10^{12})
$^{36}S^{12+}$	54	0.5[a] (3.1×10^{12})
$^{36}Ar^{12+}$	54	0.5[a] (3.1×10^{12})
$^{40}Ar^{13+}$	46	0.5 (3.1×10^{12})
$^{48}Ca^{15+}$	42	0.2[a] (1.3×10^{12})
$^{58}Ni^{19+}$	47	0.2 (1.3×10^{12})
$^{64}Ni^{20+}$	43	0.1 (6.3×10^{11})
$^{78}Kr^{24+}$	41	0.1 (6.3×10^{11})
$^{86}Kr^{24+}$	36	0.1 (6.3×10^{11})

[a] Will be available after the implementation of the U-400M upgrade in 2019.

Table 8. Main parameters of zero-angle dipole D3.

Maximum field	B_{max}	T	1.44
Minimum field	B_{min}	T	0.4
Effective length for $B = 1.2$ T	L	mm	524
Gap		mm	180
Good field region dimensions	H/V	$\pm$mm	250/75
Field homogeneity for $B = 1.2$ T	dB/B		0.003

^{17}Ne not more than 5–22%. Comparison made for the RIB intensities shows that the new setup will be by 1–2 orders of magnitude superior to the old ACCULINNA in respect to this crucial parameter.

The extension of the experimental opportunities for the new setup is foreseen. The secondary beam is transferred to a low-background area. In the vicinity of the focal plane F5 there is enough space for bulky instrumentation (zero-angle spectrometer, neutron and γ detector arrays). In particular, the zero-angle spectrometer was commissioned in 2017. This should considerably improve the cumulative energy resolution of the experiments with the observation of beam-like products or recoils. The principal parameters of this dipole magnet are listed in table 8. Experimental area at the F3-F5 zone allows further developments, including the construction of additional setups as one can see in fig. 3 and fig. 12. This should provide comfortable conditions for running at ACCULINNA-2 several experiments simultaneously. For instance, a modern technique like the MR-TOF mass spectrometer [60] together with the beam-stopping cell [61] could be installed around the focal plane F4 or F5 while the space downstream the focal plane F3 is reserved for the RF kicker. The new gas-vacuum cryogenic tools and control systems, necessary for the safe operation with gases (helium and hydrogen isotopes including tritium) at temperatures going down to 11 K [62], will be installed on the second floor at F5.

Design of the production target shown in fig. 13 provides operation with all primary beams delivered from the U-400M cyclotron (see table 7). Namely, this construction can stand up to a 2 kW power deposited in the production target by the primary beam (let's say, the ^{15}N beam with energy 49 A MeV and 6 pμA intensity bombarding the 3 mm thick Be target). To be sure about the profile of the beam spot on the production target, an originally designed monitor is installed in the diagnostic box shown in fig. 13. The monitor involves an array of secondary electron-emission grids (16 by 16 wires spaced by 1.5 mm) [63] coupled with the 32 channel readout system POLAND [64]. It can operate in a large dynamic range of intensities (10^6–10^{12} ions per second) providing a 0.5 mm space accuracy. A standard Faraday cup with a thin tantalum foil mounted on the same pneuma-input (DN100 type) is installed downstream of the target. So, one can receive permanently the data flow showing the beam current and profile obtained in front and behind the production target.

The ISOL complex of DRIBs-3 (phase 3) [65,66] will be upgraded by the reconstruction of its second-stage U-400 cyclotron. The choice of RIBs accelerated, after charge breeding, by this complex will be significantly increased, see table 9. The upgrade of the U-400 cyclotron into U-400R (letter "R" means reconstructed) will result in a considerable improvement of the beam quality and will give the RIBs with energy continuously adjustable in a range of 5–30 A MeV. The new options offered by the use of the gas cell, coupled with the RFQ cooler and buncher, and the improved system of beam extraction and shaping, implemented at the U-400R cyclotron, will expand the list of RIBs provided by DRIBs-3. Several examples of radioactive beams which will be available at the DRIBs-3 complex are listed in table 9.

4 Research program at ACCULINNA-2

The near-future goals of the research works to be done at ACCULINNA-2 are marked in fig. 14. The brief remarks given below indicate their destinations. The investigation area discussed here embraces a region of light nuclei where transfer reactions make an effective tool allowing the achievement of neutron/proton drip lines. We note

Table 9. RIBs accessible from the upgraded DRIBs-3 complex. Beam energies will be smoothly variable in a range of 5–30 A MeV. Some examples of the RIBs in a range of 3–20 A MeV available at Spiral2[a], GANIL and HIE-ISOLDE[b], CERN are given for comparison.

Facility/Beam	^{6}He	^{8}He	^{9}Li	^{12}Be	^{8}B	^{16}C	^{17}F	^{34}Si	^{46}Ar
DRIBs-3: I, pps	1×10^8	3×10^5	5×10^5	7×10^5	3×10^5	6×10^5	7×10^6	2×10^5	3×10^5
Spiral2: I, pps	3.2×10^7	3.5×10^5	2.2×10^5	6.7×10^2	3.4×10^5	–	2.1×10^5	–	–
ISOLDE: I, ppmC	5.4×10^7	6.6×10^5	3.6×10^7	7.0×10^3	3.0×10^2	4.0×10^3	1.1×10^7	–	3.0×10^4

[a] http://u.ganil-spiral2.eu/chartbeams/.

[b] http://hie-isolde-project.web.cern.ch/; http://test-isolde-yields.web.cern.ch/test-isolde-yields/.

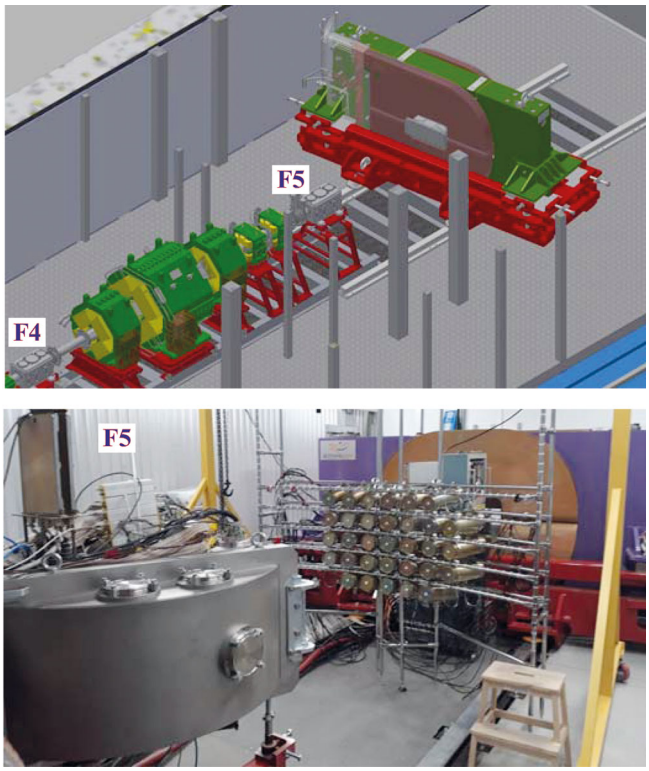

Fig. 12. Layout of experimental area around the F4-F5 planes (top) and a view of equipment in the vicinity of the final focal plane F5 (bottom).

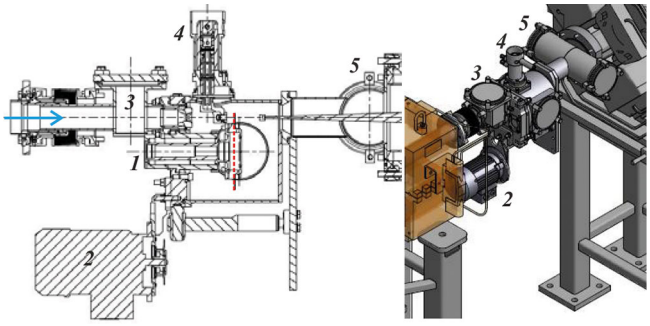

Fig. 13. Design of the production target: (1) movable water cooled unit with the Be-target disk (red dotted line); (2) motor to rotate the target unit in the range 10–50 Hz; (3) diagnostic box for primary beam profile measurements; (4) support for the diaphragms (four positions); (5) DN100 port to install a Faraday cup with a frame supporting 4 μ Ta foil.

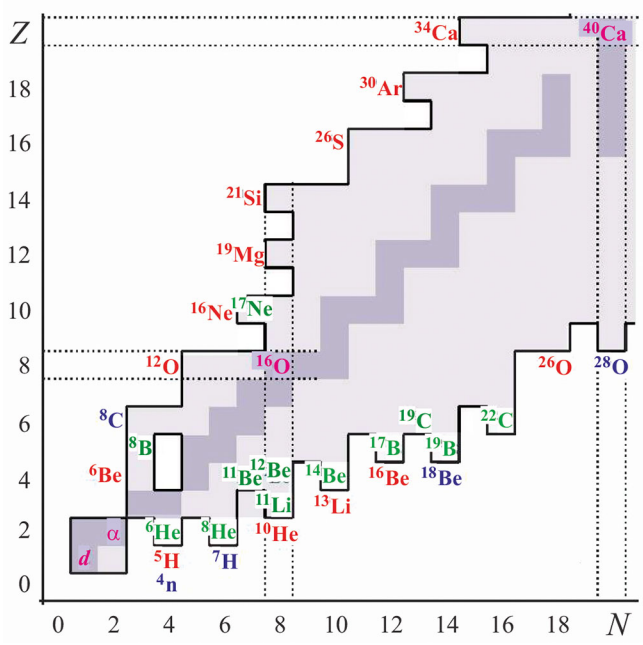

Fig. 14. The lightest nuclei on the nuclide map. The well established nucleon drip lines are presented with thick solid lines. Bluish tone shows the stability valley. Besides the doubly magic ^{4}He, ^{16}O and ^{40}Ca indicated in the drawing are the drip-line nuclei mentioned in the text.

that several research groups working at worldwide facilities [3–11] have contributed actively in the production and studies of these nuclei in the last ten years, and that further developments are expected in the next period.

4.1 Nucleon haloes, neutron skins

Weakly bound few-body exotic systems show properties very different from the nuclei which are not too far from the valley of *beta* stability. The light nuclei exhibiting one-neutron and two-neutron halo structures became the subject of intensive theoretical and experimental works. The study of the halo phenomenon is important for a better understanding of the nuclear structure close to the drip lines. Examples of known halo (skin) nuclei include ^{6,8}He, ^{11}Li, ^{11}Be, ^{14}Be, ^{17}B, ^{19}B, and ^{19}C. With the exception of

^{11}Be, which turned out to be a target for the study of the one-neutron halo, experiments could provide so far only little information about the excitation spectra of these nuclei.

Along the neutron drip line, the relatively small enhancement of the total binding occurring for paired neutrons has an important impact. Experiments giving new knowledge about the properties of the interleaving neutron-unbound nuclei should be put into the agenda of the research aimed at getting comprehension about the character of neutron-nucleus interaction far from stability, coupling to the continuum in neutron-rich systems, and delicate structures inherent to the multi-neutron haloes or skins. Studies of the adjacent neutron-unbound (odd-N) nuclei could yield information on the nucleon orbitals important for the description of the heavier bound nuclei. With regards to the drip-line nuclei of beryllium, boron and carbon specifically interesting are the spectra of ^{13}Be, ^{16}B, ^{18}B, and ^{21}C.

The search for resonant states in the unstable nucleus ^{13}Be has been going on since the eighties. Recent papers report on the resonant states of ^{13}Be obtained by means of the invariant mass method via the one-two nucleon removal ^{1}H(^{14}Be, ^{12}Be+n+X) [67,68], ^{12}C(^{14,15}B, ^{12}Be+n+X) [69], and nucleon-exchange ^{9}Be(^{13}B, ^{12}Be+n+X) [70] reactions. References to the earlier experiments are made in these papers. Resonant states of ^{16}B were studied by means of a multi-nucleon transfer ^{14}C(^{14}C,^{12} N)^{16}B [71] and neutron-proton removal ^{12}C(^{17}C, ^{15}B + n + X) [72] reactions. The spectrum detected in both papers showed a low-lying level in ^{16}B. The authors of ref. [73] reported on ^{18}B obtained in the ^{9}Be(^{19}C, ^{17}B + n + X) reaction. The measured decay-energy spectrum of ^{18}B showed an s-wave shape. An upper limit for the scattering length was found to be -50 fm. From the spectrum obtained in the ^{9}Be(^{17}C, ^{15}B + n + X) reaction these authors came to the conclusion that the results obtained for ^{16}B are similar to those reported in [71,72]. A tentative measurement of the ^{21}C decay spectrum was reported in ref. [74], it was obtained using the single-proton removal reaction from the ^{22}N beam at 68 A MeV.

Nucleon knockout and the more conventional transfer reactions are complementary approaches for this case. While knockout reactions mainly probe hole strengths, the nucleon transfer reactions like (d,p), (t,d), (t,p) and $(^3\mathrm{He},d)$ populate particle orbitals. Adding to the arsenal the nucleon pickup reactions from the RIB projectile nuclei, *e.g.* reactions of the $(d,{}^3\mathrm{He})$, (p,d), and (p,t) types, one can populate nucleon-hole states in exotic nuclei. The orbital angular momentum quantum numbers, the relative location of single-particle states, and spectroscopic factors are accessible in experiments employing direct reactions. Transfer reactions access many excited states simultaneously, and their strong kinematic matching allows the optimum choice of reactions populating the nuclear states with orbital angular momentum of the interest. Nucleon transfer and charge-exchange reactions, such as (p,n) and $(t,{}^3\mathrm{He})$, offer a robust way to perform through studies of the halo nuclei.

4.2 Exotic multi-neutron decays (2n virtual states, 2n and 4n radioactivity)

Beyond the drip lines, we get at the regions of strong nuclear instability. Here, in the region of light neutron-rich nuclear systems, the experimental observations could be especially confusing. In the absence of strong potential barriers the observables becoming typical for the neutron decays, are often sensitive to the reaction mechanism. Also, the appearance of novel dynamics forms is not impossible here. These include the possible existence of hypothetical two-neutron virtual states [75] and two/four-neutron radioactivity [76]. The search for the few-neutron radioactive decays is inspired by the discovery of the two-proton radioactivity [77,78]. In contrast with the situation coming across near the proton drip line, the long-lived one-neutron emitters are practically impossible, while the $2n$ and $4n$ emitters may have quite long lifetimes, even falling in the radioactivity timescale. The discovery of such a novel type of radioactive decay is a challenging task requiring elaborate experimental approaches. At present time, the studies of nuclear systems with large neutron excess are active in different centers having intermediate-energy RIBs. Different authors published the results of their experiments devoted to the studies of the true two-neutron emitters ^{10}He [33, 36, 79–82], ^{13}Li [83, 84], ^{16}Be [85, 86], and ^{26}O [87–91].

Examples of successful experiments dedicated before to the exploration of the topics of $1n$ and $2n$ emitters beyond the neutron drip line, are the studies of neutron decays of some states in ^{5}H, ^{8}He, ^{9}He, and ^{10}He. Refined data on the ^{3}H(^{8}He, p)^{10}He reaction, obtained at the ACCULINNA separator [36], confirmed the results reported in ref. [33]. The new data positioned the ^{10}He ground-state resonance at 2.1 ± 0.2 MeV above the threshold of the three-body ^{8}He+n+n decay and revealed the onset of intruder states and changing the spin-orbital interaction as prominent shell-breaking effects in the ^{10}He spectrum. The extension of these works to similar systems is foreseen. The excitation spectra of ^{7}H, $^{11-13}$Li, $^{13-16}$Be, $^{16-19}$B etc. will be a first-priority task for ACCULINNA-2. The study will include precise determinations of ground-state masses made for these nuclei. It is worth noting that currently none of the neutron separation energies is known to better than 10 percent for these nuclei. Transfer reactions of the (t,p) and (d,p) type, studied in inverse kinematical conditions, are the most suitable ones for the precise mass measurements. High statistics data will be accessible for complete kinematic measurements performed for the resonant states of these little-studied nuclei.

4.3 Soft excitation mode

The idea of neutron halo became the starting point for the prediction of a low-lying dipole excitation mode, *i.e.* the so-called soft dipole mode [92]. Its appearance is connected to the suggested low-frequency oscillations of the halo neutrons against the core, giving rise to low-lying dipole excitations. Assuming this hypothesis, large

electromagnetic dissociation (EMD) probability was predicted [93] for ^{11}Li incident on heavy targets. The large cross-sections expected for the Coulomb dissociations of the Borromean halo nuclei have been confirmed experimentally (see *e.g.* [94]). It should be noted that, at least for the lightest Borromean halo-nuclei ^{6}He and ^{11}Li, the low-lying dipole excitations are not resonant ones (these are rather ordinary low-lying continuum states). However, it does not mean that these states cannot have resonant character in other halo nuclei.

The study of the soft mode showing up in the ^{8}He spectrum, performed in [34, 35], demonstrates how deep one can get into the mechanism of this excitation created by the low-frequency oscillations of the halo neutrons against the nuclear core. In particular, the possible nature of the near-threshold anomaly above 2.14 MeV in the ^{8}He missing mass spectrum was explained by the population of a 1^- continuum (soft dipole excitation) with a peak energy value of about 3 MeV.

High precision and high statistics data on the three-body $\alpha+p+p$ continuum of ^{6}Be were obtained recently in the charge-exchange $p(^{6}\mathrm{Li}, ^{6}\mathrm{Be})n$ reaction [38]. The ^{6}Be excitation-energy (E_T) spectrum was explained by the population of three main structures in ^{6}Be, *i.e.* the 0^+ state at 1.37 MeV, the 2^+ state at 3.05 MeV, and a mixture of 0^-, 1^-, 2^- continuum in the E_T extending from 4 to 16 MeV. The negative-parity continuum was interpreted as a novel phenomenon, the isovector non-resonant soft dipole mode.

Transfer and charge-exchange reactions, studied at beam energies of 20–40 A MeV grant excellent conditions for such research.

4.4 New magic numbers and intruder states

There are basic problems in the field of exotic nuclei where ACCULINNA-2 will provide favourable conditions to be studied in detail. One example is the ascertainment of the patterns associated with the closed-shell breakdown at the magic neutron number $N = 8$ and the manifestation of s-d intruder states in the neutron-rich nuclei ^{9,10}He, ^{10,11}Li, ^{11,12}Be. Clarification of filling sequences arising in the s-d neutron shell in a number of neutron-excess nuclei (*e.g.* ^{15}Be, ^{16,18}B, ^{17,19}C) and the interplay of s- and d-wave states in their even-N neighbours is another basic problem, which calls for thorough investigation. On the proton-excess side, similar phenomena call for the study of the possible two-proton halo structure, with a ^{15}O core, predicted by theory for ^{17}Ne. Of special interest is the termination of the s-d shell occurring in the C, N, O, F and Ne nuclei in the vicinity of neutron number $N = 16$. The 20–30 A MeV beams of ^{24}O, ^{26,27}F, ^{28,29,30}Ne offered by ACCULINNA-2 provide good conditions for the study of resonant states of nuclei (*e.g.* $^{24-26}$O) lying near and beyond the drip line.

4.5 Two proton radioactivity

The upgrade of the U-400M cyclotron planned for 2019 will open ways to the whole series of proton-rich nuclei with $Z \leq 36$, lying close and beyond the proton drip-line. These include a number of nuclei predicted to exhibit $2p$-radioactivity. Furthermore, the $2p$ decay of resonant states gives rise to a profound interest in the dynamics of this decay mode. Clear examples to be studied are the resonant states of ^{6}Be, ^{12}O, ^{16}Ne, ^{26}S, ^{30}Ar, ^{48}Ni etc. The finding and measurement of the $2p$-decay branch for the first excited state of ^{17}Ne will clarify the issues related to the $Z = 8$ waiting point affecting the rp-process in the sites of hot stellar burning.

The proton drip line is quite well known for nuclei with $Z \leq 36$. Only a few isotopes, remaining unknown here, could exist showing half-lives comparable with the time-of-flight through the fragment separator. Recently, the ACCULINNA group performed dedicated search for the drip-line nucleus ^{26}S produced in fragmentation of ^{32}S beam nuclei [42]. A half-life limit of $T_{1/2} < 79$ ns was set for ^{26}S in this study. Another example is ^{48}Ni which was studied in 2011 by means of an imaging time projection chamber [95]. As a result, for the first time a $2p$ decay branch was observed and the half-life of ^{48}Ni was determined to be 2.1 ms. The properties of the neighbor nuclei ^{21}Si, ^{30}Ar and ^{34}Ca with half-lives shorter than 100 ps can be ascertained well due to the excellent choice of RIBs provided by the ACCULINNA-2/U-400M complex. In particular, the rare phenomenon of the β-delayed $3p$-decay of ^{31}Ar [96] could be investigated in more detail. The quest for ^{21}Si and ^{26}S is challenging because it is very probable that the two-proton emission is the main decay mode of these nuclei. Quite detailed studies of the $2p$ decay mode will be feasible for the nuclei having life-time $T_{1/2} > 50$ ps. This becomes realistic because one can produce these nuclei in transfer reactions induced by the ACCULINNA-2 RIBs. The (p, d) and (p, t) type reactions are favorable to cope with this task. For the searched nuclei, their formation and decay, occurring in-flight, should be established by the detection of the daughter nucleus and the two emitted protons. The decay time is derived from the distance between the target and the vertex position defined as the intersection point of the momentum vectors of the two emitted protons with the daughter-nucleus trajectory.

The suggested approach works well also when the $2p$-decay life times are very short with the lower limit coming close to the characteristic nuclear time. This is true for the excited states of the searched $2p$ emitters. Precision measurements of the $2p$- and p-decay characteristics made for a dozen of nuclei with $Z \leq 36$, lying beyond the proton drip line, should be included in the research program.

4.6 Spectroscopy of exotic nuclei

A notable series of works carried out at ACCULINNA was accomplished with the application of correlation techniques in the studies of transfer reactions resulting in the population of excitation spectra in exotic nuclei. In

a somewhat less general form such technique was applied before to the spin-parity identification of excited states displaying the emission of spinless particles. In the experiments performed at ACCULINNA, the method was further developed [29, 30] and its applicability was demonstrated in some works [29–42]. The point is that highly aligned states are produced in the direct reactions. In the rest frame of the exotic nucleus, formed as the reaction product, the highest degree of spin alignment is obtained in respect to the axis parallel to the transferred momentum vector. If one is lucky, the decay of the aligned configuration may produce sharp correlation patterns. If one is lucky even more, the interpretation of the observed correlations may appear to be unique, this was the case, for example, with the spectrum of ^{9}He populated in the (d, p) reaction [32]. This "unstable" aspect of this approach depends on such details of reaction mechanism and spectral densities of different states which one cannot predict in advance.

Typically, the resonance states of light drip-line nuclei (especially on the neutron-excess side) are broad and overlapping, and their correlation patterns are affected by interference. Therefore, even weakly populated states may become apparent due to the contribution made into the interference patterns. The addition of amplitudes acts in this situation as a kind of "quantum amplifier" giving access to the details of the spectrum which otherwise would be too complicated for their revelation. Benefits derived from the correlation aspect of spectra populated in direct transfer reactions are always implied in the consideration of the ACCULINNA-2 research program.

4.7 Cluster states

In proximity to the decay thresholds some nuclear states possess expressed cluster structures, and new forms of nuclear dynamics arise. Such states have been found, for example, in Be isotopes —the observed excited states form rotational bands with a well-expressed molecular structure, characterized by large deformation. Good candidates for such studies are the heavy isotopes of He, B, C, O, Ne, etc.

The correlation measurements and the complete kinematics studies, discussed above, form the most common way for elucidating the clustering aspect of nuclear dynamics. The importance of the Optical Time-Projection Chamber [48, 49, 95–97] should be specially emphasized here. It gives the opportunity to make complete kinematics measurements in experiments where the "useful" counting rates are just units and tens of events. This is important for the studies of exotic nuclear systems attainable with low production rates.

A number of related experiments was performed with OTPC at ACCULINNA [48,49,97]. Evidence produced for the neutron emission after the β-decay of ^{8}He to a highly excited ^{8}Li state indicates that the early reported decay scheme of ^{8}He is not complete. The methods making use of OTPC offer unique opportunities for the study of rare decay branches of excited ^{8}He nucleus in, *e.g.*, the α+t+n, ^{7}Li + n, ^{6}He + d [49] and beta delayed one-, two-proton emission of ^{26}P, ^{27}S [97].

Another field for the cluster structure-studies concerns the states in ^{6}He with a $t + t$ structure and a possible ^{5}H + t clustering of ^{8}He. Reactions of quasi free scattering (QFS) are sensitive specifically to the clustering aspect of the nuclear structure. In this class of reactions, the selection of a quasi free knock-out channel explicitly defines the clustering partition of the studied nucleus. The quasi free scattering reactions reported in ref. [24] could be effectively applied for the further determination of the halo structures in ^{6}He, ^{8}He and other exotic nuclei. While typically the valence nucleon is knocked out in the QFS, the $(\alpha, 2\alpha)$ knock-out of the halo nucleus ^{6}He core was examined in [24] elucidating different aspects of the nuclear structure.

4.8 Reactions with halo nuclei

Fusion reactions detected with the beams of halo nuclei have been of increased interest from experimental and theoretical points of view. In particular, much effort has been devoted to the subject of near-barrier fusion of light, weakly bound projectile nuclei. Unusual effects are expected here both from the halo structure of these nuclei and from the specific tunneling mechanism of the composed weakly bound system which is of general interest for the quantum theory. One example of this type of effects represents the recent study of the fusion reaction ^{6}He+ ^{206}Pb carried out at DRIBs-3 [98]. Another example is the study of complete and incomplete fusion reactions of ^{6}He and ^{6}Li projectiles with ^{165}Ho and ^{116}Er target nuclei [99]. The upgraded DRIBs-3 complex will give higher intensity and higher quality beams of ^{6}He nuclei and also a variety of other exotic beams (^{8}He, ^{9}Li, ^{12}Be, etc., see table 9) thus offering prospects for new insights into the process of low-energy fusion and multi-nucleon-transfer reactions of light exotic nuclei hitting against heavy targets.

4.9 Astrophysical applications

Nowadays, the nuclear astrophysics research is an integral part of the novel forms of nuclear dynamics studies. The finite nuclear matter is the only directly accessible "testing ground" for theoretical models that are meant to look into the states of the infinite stellar matter. The following data are required:

i) masses and level schemes close to the neutron, proton, and alpha breakup thresholds;

ii) significance of electron capture for determining the β-decay lifetimes;

iii) partial proton, neutron, α, γ widths of low-lying resonances necessary for calculating the resonant radiation capture and (n, α) or (α, n) reaction rates;

iv) electromagnetic E1 and E2 strength functions to calculate the non-resonant radiation capture, extracted from the data on the electromagnetic dissociation of the corresponding nuclei.

Nuclear reactions in stars involve short-lived proton-rich and neutron-rich nuclei that can be studied only with radioactive beams. The cross-sections of interest have to be obtained indirectly by the study of resonance reactions made in inverse kinematics on the hydrogen and helium target nuclei and by means of transfer reactions allowing one to determine the level schemes and spectroscopic properties of nuclear states. This includes peripheral transfer reactions known to be suitable to measure the quantities called Asymptotic Normalization Coefficients (ANCs), determining stellar capture rates. Transfer reactions performed with the RIBs delivered by DRIBs-3, such as (d, n), (d, p), (t, d), (p, d), or $(^3\mathrm{He}, d)$ can be used to extract the proton spectroscopic factors, ANCs, or neutron spectroscopic factors in mirror nuclei.

Although, in general, the highest possible incident beam energies are preferable for the Coulomb dissociation reaction studies, for low-energy beams anticipated in the presented DRIBs-3 project a list of relatively low energy (*e.g.*, at energies of 50 A MeV and below) studies exists for the drip-line nuclei. The low-energy case is more challenging from the theoretical point of view and requires more theoretical contribution for data interpretation. However, problems arising here are known to be tractable. Coulomb dissociation cross-sections are straightforwardly related to the rates of the astrophysical non-resonant radiation. The Coulomb dissociation reactions and, *e.g.*, transfer reactions populating continuum states could be also regarded as the representatives of a broader class of the processes capable of elucidating the continuum excitation properties. An interesting possibility is to study the breakup reactions in complete kinematics for the breakup products. Breakup processes on light targets can be considered as alternative to the Coulomb dissociation reactions. They are characterized by strong Coulomb nuclear interference and could be much more complicated for interpretation. However, such reactions have different selectivity in quantum numbers compared to the Coulomb dissociation, which almost exclusively populates E1 and E2 states. A good example is the issue of actively discussed three-body virtual states. The ground states of ^{10}He and ^{13}Li could be such three-body virtual states. Just as it occurs with ordinary two-body virtual states, these objects resemble rather the final state interactions than the real resonance states characterized by a compact size and a definite lifetime.

Two-proton radiative capture is a process whose importance along the *rp*-process path has been poorly understood so far. This process is directly related to two-proton radioactive decay. This means that limited information about $2p$ radioactivity and all complexities of this phenomenon are projected to this field as well. A particularly important region that will become accessible to experiments is that around the critical waiting points ^{64}Ge, ^{68}Se, and ^{72}Kr. These waiting points shape the light curves of the X-ray bursts and determine the amount of heavier nuclei produced. Another case important for the passage of the *rp*-process is the ^{15}O waiting point. The fact that the two-proton capture is a possible alternative to the (α, p) reaction as a pathway for the *rp*-process makes topical the search for a weak $2p$ decay branch of the first excited $3/2^-$ state in ^{17}Ne. Such a search carried out at a level of $\Gamma_{2p}/\Gamma_\gamma \sim 10^{-5}$–$10^{-6}$ predicted by theory [43] but still not checked experimentally [44–47] will be feasible with the use of intense $Z = 8$–10 radioactive beams provided by DRIBs-3.

5 ACCULINNA-2 status

The technical launch of the ACCULINNA-2 facility was carried out in December 2015. The primary beam of ^{32}S with energy 51.5 A MeV was transported to the F2 focal plane, and the beam characteristics were examined using a set of Faraday Cups (located along the line from the U-400M output up to F2) and a couple of Al_2O_3 luminophores located at the focal planes F1 and F2. The beam transmission from U-400M to F1 and from F1 to F2 made more than 90 and 98 percents, respectively. These values, together with the size and the beam profile observed in F2, are in excellent agreement with the simulations and fully meet the requirements of the project [14, 15]. The design and construction works of a new cabin were performed in 2016. This is intended for housing the linear part of ACCULINNA-2, extending from the plane F3 to F5, and providing enough space for the placement of the reaction chamber, the zero-degree magnet, and the neutron array together with its 6-meter flight path. In 2018 the ACCULINNA-2 setup will be put into the full-scale operation assuming the availability of the complete set of instruments involving i) hodoscope detectors for the zero-angle spectrometer; ii) the RF-kicker installation and switching on; iii) significant reinforcement of the radiation protection around the production-target area F1-F2.

The first operation tests of the ACCULINNA-2 separator were done with the primary beams delivered from the U-400M cyclotron with intensity limited at a level of no more than 100 pnA. The reason for such limitation was an open space around the F1-F2 area, *e.g.* we did not have any concrete shielding there. Calculations of radiation dose, emerging at working conditions inside and outside the cyclotron hall, were made with the use of code FLUKA [100,101]. As a result, parameters were chosen for the concrete shielding enclosing the area between the F1-F2 focal planes. Together with the 2-meter thick walls of the cyclotron hall, this protection will provide radiation-safe conditions outside the hall area even at a 4 pμA primary beam intensity, see fig. 15. The expected level of neutron background, the main danger factor for man, will be around 10 μSv per hour, or even smaller, outside the green walls (top panel in fig. 15). So, the primary beams listed in table 7 will be available for experiments since the fall 2018.

5.1 First radioactive beams

The first radioactive ion beams at ACCULINNA-2 separator were produced in March 2017. The primary beam

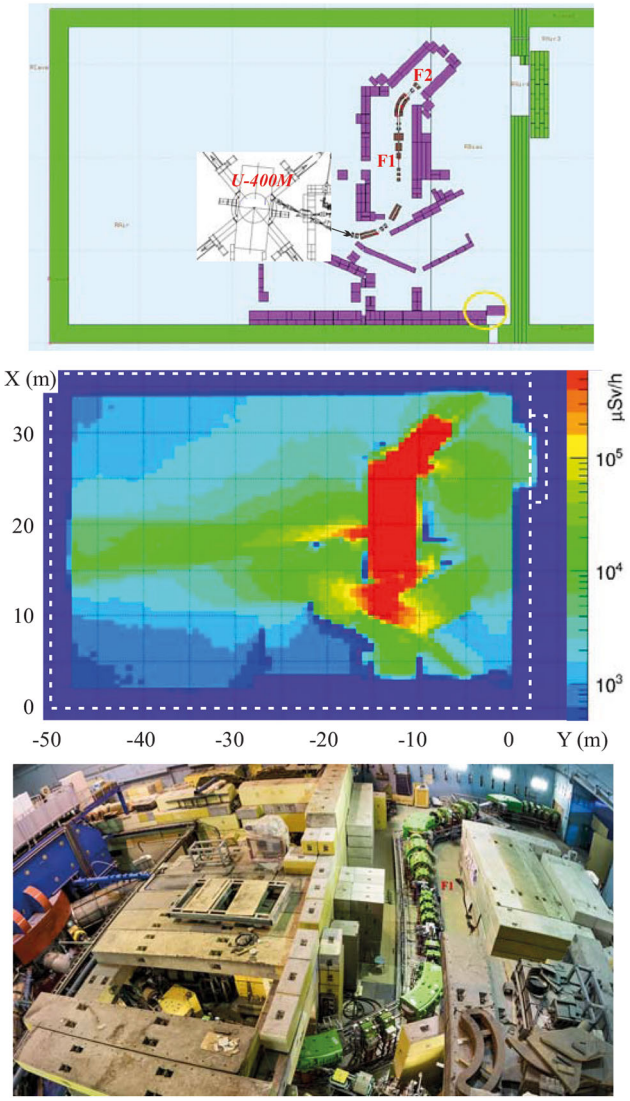

Fig. 15. Top panel: the concrete walls of the cyclotron hall (green) and the concrete shielding (violet) enclosing the area between the F1-F2 focal planes. Middle panel: the calculated pattern of radiation dose obtained inside the cyclotron hall and outside (*i.e.* outside a white dotted line) in the beam-line plane situated at a level of 120 cm above the floor. The case is shown where a ^{15}N beam (beam energy 49.7 A MeV, current 4.0 pμA) hits a 2 mm Be target, and the separator is tunned for giving the ^{8}He RIB. The top view of the setup inside the cyclotron hall, bottom panel.

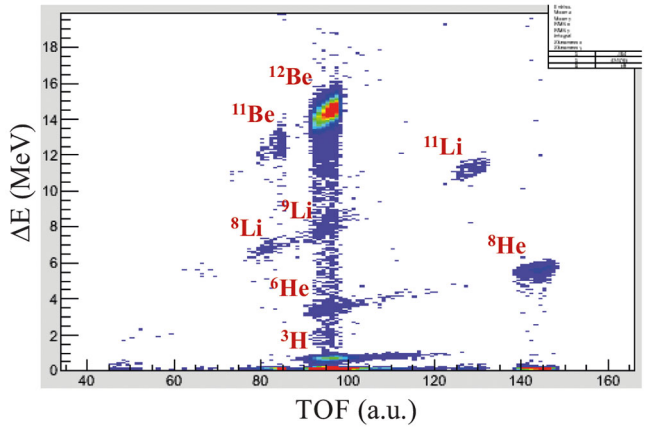

Fig. 16. RIBs identification plot in the F5 plane when the separator was tuned to the ^{12}Be beam with energy 39.4 A MeV from the reaction ^{15}N (49.7 A MeV) + Be.

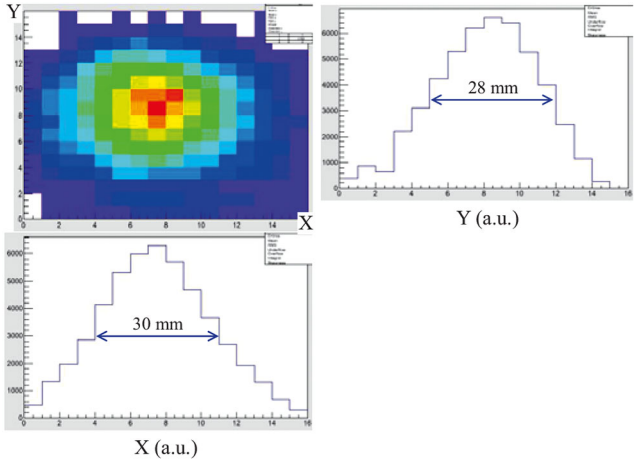

Fig. 17. Beam profile of ^{12}Be ions in the final focal plane F5 measured by the position-sensitive silicone detector. The size of one bin is 4 mm.

of ^{15}N with energy of 49.7 A MeV was delivered to the F1 focal plane where the 2 mm thick beryllium production target was located. In all measurements a 1 mm beryllium wedge was installed in the dispersion focal plane F2. The products of beam fragmentation were registered by the system of RIB diagnostics consisting of a TOF and energy loss detectors. The TOF array involved a couple of plastics (BC404) housed in the round-form frames. The thickness of each scintillator was 0.25 mm, and the diameter of the sensitive area was 60 mm. Each scintillator was coupled with four Hamamatsu R7600 photomultiplier tubes. The TOF detectors were located at the F3 and F5 focal planes. The 0.3 mm thick double-sided strip silicon detector (Micron-Semiconductor, type BB7) with sensitive area 64 by 64 mm, and with 32 strips on each side, was located behind the second TOF detector in the F5 plane. Similar BB7 detectors were used for the measurement of energy losses and beam profile in the focal planes F3 and F4.

The typical two-dimensional identification plot, the energy loss ΔE *versus* TOF, obtained for the final focal plane F5 when the separator was tuned to the ^{12}Be ions with energy 39.4 A MeV, is shown in fig. 16. The pattern shown there was obtained for the momentum acceptance of ±2%. In this case the purification of the ^{12}Be beam was

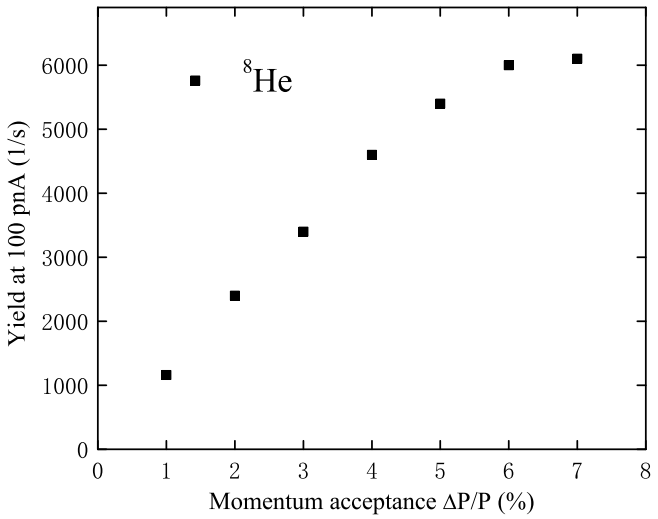

Fig. 18. Dependence of the ^{8}He yield on the momentum acceptance of ACCULINNA-2 measured in the final focal plane F5 and normalized for the 100 pnA ^{15}N primary beam.

Table 10. Main parameters obtained for several light neutron-rich RIBs in final focus F5 when a 49.7 *A* MeV ^{15}N with the intensity of 100 pnA bombarded a 2 mm beryllium target. Data were obtained for the momentum acceptance of ±2%, beryllium wedge 1 mm thick (F2) and ±11 mm slits in F3.

RIB	^{14}B	^{12}Be	^{11}Li	^{9}Li	^{8}He
Energy, *A* MeV	37.7	39.4	37.0	33.1	35.8
Intensity, 1/s	1.2×10^4	1.5×10^4	4×10^2	1.1×10^5	2.5×10^3
Purity, %	65	92	67	51	89

around 90 percent, in agreement with calculation results. The beam profiles at the F3-F5 planes were obtained being in accord with the typical calculations shown in fig. 10. In particular, the ^{12}Be beam spot at F5 was defined as X ∼ 30 mm (FWHM) and Y ∼ 28 mm (FWHM) when all multipoles were switched off, see fig. 17. Operation with the multipoles being switched on resulted in a little bit narrower horizontal size X ∼ 27 mm (FWHM) with the same vertical distribution. The result is also in agreement with the calculation.

The basic RIB parameters, energy, intensity and purity, obtained for several neutron-rich isotopes from the reaction ^{15}N (49.7 *A* MeV)+Be (2 mm) are listed in table 10. In these measurements the intensity of the primary ^{15}N beam was limited to 100 pnA. A 7 mm the cross-sectional dimension was assured for the beam spot obtained on the production target in plane F1. The obtained RIB intensities were close to the results of calculations made with the use of the LISE++ [102] code. The calculations show that the RIB intensities obtained in the F5 plane can be enlarged by ∼ 2.5 times by making the cross-section of the primary beam equal to 4 mm when it hits the production target in the F1 plane. Another point being important for the RIB production rate and beam purity is the dependence of these values on the momentum acceptance defined by the size of the slit placed in the wedge front in the focal plane F2. This was checked experimentally, and the result obtained for the ^{8}He case is shown in fig. 18. The maximum intensity obtained for the ^{8}He beam at the ±3% momentum acceptance is obviously seen in this diagram. This result is in accordance with our expectations.

5.2 Day-one experiments

We are convinced now that the ACCULINNA-2 separator will give high quality secondary beams, and this opens new opportunities for experiments carried out with RIBs in the intermediate energy range 10–50 *A* MeV. Other advantages of the new facility equipped with the zero-angle spectrometer and RF kicker will be important in many cases. The benefits given by the full-scale facility are necessary to carry out first-priority experiments, in particular, for the study of the ^{7}H, ^{10}He, ^{16}Be, ^{17}Ne and ^{26}S nuclei. The program of the earliest experiments at ACCULINNA-2 was extensively discussed at EXON conferences since 2014 [103, 104], and some proposals have been specified [39,46,60,105–107]. In particular, the study of isotopes ^{7}H, ^{17}Ne and ^{26}S are in the sphere of top-priority interests.

Attempts to observe the ^{7}H ground-state resonance produced in different reactions were undertaken repeatedly [108–112], but the reported results were not convincing. Only the authors of the most consistent and sensitive experiment [111] could pretend that they have some indication for the observation of low-lying ^{7}H resonance in the missing-mass spectrum obtained in the ^{2}H(^{8}He,^{3} He)^{7}H reaction. Having a poor experimental resolution attained in this work (∼ 1.5 MeV), the authors observed a peculiarity at ∼ 2 MeV populated with a cross-section of about 30 μb/sr. More statistics and better energy resolution are obviously needed in such kind of measurements to observe a narrow ^{7}H resonance in accordance with the expectations given in ref. [39].

The layout of a setup presented in fig. 19 illustrates the concept which could be realized in experiments intended for the revelation of the ^{7}H ground-state resonance populated in any of the two transfer reactions: ^{2}H(^{8}He,^{3} He)^{7}H or ^{2}H(^{11}Li,^{6} Li)^{7}H. Basically, this concept is similar to that employed in the cited work [79]. But in addition to the missing-mass measurement, the setup shown in fig. 19 is optimized to deliver information about the correlations inherent to the ^{7}H decay products. Besides the detection of the recoils emitted in the reactions chosen for the study (the ^{3}He or ^{6}Li recoils are assumed to be recorded in these

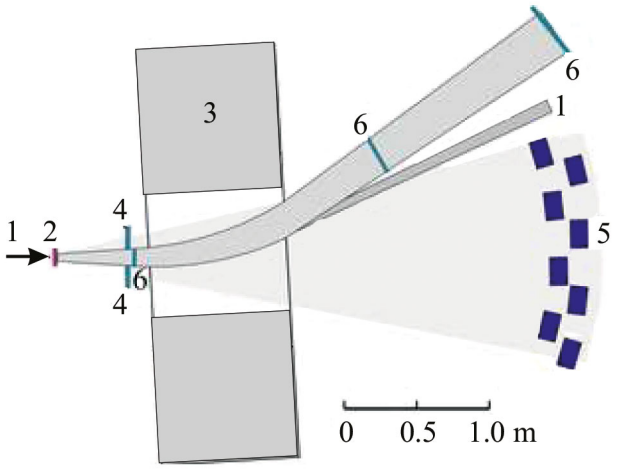

Fig. 19. Layout of the setup to be used for the study of the ^{7}H excitation spectrum which could be populated in the transfer reactions ^{2}H(^{8}He,^{3} He)^{7}H or ^{2}H(^{11}Li,^{6} Li)^{7}H. Numbering means: (1) RIBs, (2) deuterium target, (3) zero-angle dipole magnet, (4) telescopes detecting ^{3}He or ^{6}Li recoils, (5) array of stilbene crystals for neutron detection, (6) array of hodoscopes for coordinate detection of tritons emerging from the ^{7}H decay.

reactions, respectively) the decay products of ^{7}H, the triton and neutrons, will be detected by the setups. The energy of the projectiles $\sim$ 30–35 A MeV is optimal to reach the maximum cross-sections available for the reactions being notable for their rather large negative Q-values. The beam intensities are enough to keep luminosity at a level of $\sim 10^{26}$ cm^{-1} s^{-1} having the deuterium targets thin enough for getting at $\sim$ 500 keV energy resolution in the measured missing-mass spectra. Hodoscopes placed in three planes along the charged particle trajectories will give information defining the momentum vectors of tritons detected in coincidence with the recoils. The wide aperture of the magnet allows the tritons and neutrons, emitted from the deuterium target, to pass with minimal losses to the respective detector arrays. The array of stilbene crystals [53] will provide about 15 percent detection efficiency for the neutrons emitted at the decay of a low-lying resonance state obtained in ^{7}H. As a result, $\sim$ 20 events per day are expected to be recorded in the case that the reaction cross-section makes 30 μb/sr for the ^{7}H system formed with the missing-mass energy below 2 MeV.

Another hot problem appearing to be an immediate task addressed to the enhanced ACCULINNA-2 capabilities is the unsolved conundrum of the possible two-proton decay of the first excited state of ^{17}Ne [39,47]. The energy of the 1288 keV ^{17}Ne first excited $3/2^{-}$ state exceeds the threshold of $2p$ emission by 344 keV, and the single-proton emission from this state is not allowed. Therefore, the true two-proton decay might be possible if this $2p$ decay branch of this excited state could compete with gamma decay. The experimental measurement of the $\Gamma_{2p}/\Gamma_{\gamma}$ width ratio for this excited state is of considerable interest because the reverse process of simultaneous two-proton capture could be a bypass for the ^{15}O waiting point occurring in the CNO cycle of nucleosynthesis [113].

Searches for the $2p$ decay mode of this ^{17}Ne state gave an experimental limit of $\Gamma_{2p}/\Gamma_{\gamma} \leq 7.7 \times 10^{-3}$ [44, 45], while the theory work [43] predicts a value of $\Gamma_{2p}/\Gamma_{\gamma} \sim 10^{-5}$–$10^{-6}$ for this ratio. A novel approach suggested and realized in ref. [46,47] made possible to lower this ratio to a level of $\leq 1.6(3) \times 10^{-4}$. A key stone of the carried out measurements was the so-called combined-mass method applied to the investigation of the ^{17}Ne excitation spectrum populated in the $p(^{18}\mathrm{Ne}, d)^{17}$Ne reaction. Having the emission angle of the recoil deuteron measured even with a modest accuracy (about one degree) one determines with a tremendous accuracy (energy and angular resolution better than 100 keV and 0.1 degree, respectively) the energy and escape direction of the center of mass of ^{17}Ne in a lab system. The resolution, becoming attainable when the recoil deuteron, coming from the $p(^{18}\mathrm{Ne}, d)^{17}$Ne reaction, is detected in coincidence with the proton pairs emitted by ^{17}Ne, depends on the target thickness which can be set to be quite large due to the small specific energy losses of the protons having quite a large energy in a lab system. This favors the revelation of such a small $2p$ decay branch as it is anticipated for the 1288 keV excited state of ^{17}Ne.

Some perfection of the detector array, used for the measurements done in the combined mass method, could give good prospects for achieving this objective. The grounds for this conclusion were checked by Monte Carlo (MC) simulations, see fig. 20 and ref. [47]. The prime parameters of the setup which affect the energy resolution are the target thickness, energy, and angular resolutions of the charged-particle telescopes. The optimized setup will have a gaseous hydrogen target with a thickness of 1.2 mg/cm^2. A supposition is made that the used recoil-deuteron detector array will ensure measurements done for the reaction $p(^{18}\mathrm{Ne}, d)^{17}$Ne in angular range 8–24 degrees in the center-of-mass system. So, a considerable reduction of the $\Gamma_{2p}/\Gamma_{\gamma}$ upper limit (one order of magnitude and more) looks possible without revolutionary modification of the setup. This will open a way to the direct experimental observation of the true radioactive $2p$ decay of the first excited state of ^{17}Ne taking the theoretically predicted $\Gamma_{2p}/\Gamma_{\gamma}$ ratio [43].

A setup like that which is shown in fig. 19, relevant to the ^{7}H experiments, could also be applied for the observation of the short-lived ^{26}S isotope [42] produced in the two-neutrons transfer reaction $p(^{28}\mathrm{S}, t)^{26}$S. The points of difference are the hydrogen target, the recoil triton, and the three charged particles, $p + p + {}^{24}$Si, assumed to be emitted at the ^{26}S decay. Compulsory for these experiments is the availability of the RF kicker needed for the RIB purification for the case of the ^{28}S projectile, see fig. 11 as an example. Taking a typical level of $\sim 200\,\mu$b/sr, estimated for the reaction cross-section, and assuming that a 1 mm thick liquid-hydrogen target is bombarded by 35 A MeV ^{28}S nuclei with intensity $\sim 10^{3}$ s^{-1}, one could expect around 10 events per week observed for a narrow resonant state of ^{26}S.

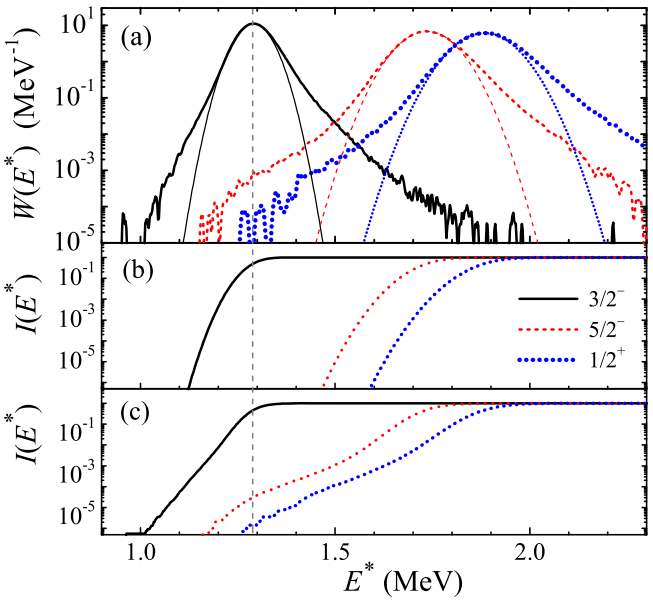

Fig. 20. MC simulations of the improved setup demonstrating the potential of the combined-mass method for achieving a level of $\leq 1.0 \times 10^{-5}$ for the width ratio $\Gamma_{2p}/\Gamma_\gamma$ of the first $3/2^-$ excited state of ^{17}Ne populated in the $p(^{18}\mathrm{Ne}, d)^{17}\mathrm{Ne}$ reaction. The normalized to the unity probability density $W(E^*)$ distributions are shown with the thick curves in panel (a) for the three resonance states of ^{17}Ne situated above the decay threshold at energy E^* 1.288 MeV ($3/2^-$), 1.764 MeV ($5/2^-$), 1.916 MeV ($1/2^+$). Thin curves in this panel give the Gaussian fits made to the obtained probability distributions. Panels (b) and (c) demonstrate the cumulative distribution function I for the Gaussian fits and for the complete MC distributions, respectively. As the $5/2^-$ state of ^{17}Ne is weakly populated in the $p(^{18}\mathrm{Ne}, d)^{17}\mathrm{Ne}$ reaction, the limit achievable for the searched $\Gamma_{2p}/\Gamma_\gamma$ ratio should be estimated taking the background appearing at $E^* = 1.288$ MeV from the two-proton decay of the $1/2^+$ state at 1.916 MeV.

6 Prospects for the period 2018–2023

The arrangement of conditions required for carrying out experiments intended for the work with cryogenic tritium targets is the chief task being performed at present. Substantial prospects are offered by the implementation of this technique for the study of nuclei in the vicinity of the neutron drip line. Two-neutron transfer reactions induced by RIBs hitting a cryogenic tritium target were proved to be an effective tool in the study of the drip-line, neutron-rich nuclei ^{5}H, ^{8}He, ^{9}He, ^{10}He (*e.g.* see in [30,36]). The combined-mass method, for the first time realized in work [47], done on the first excited state of ^{17}Ne, offers good possibilities for the systematic study of excitation spectra of nuclei residing in the vicinity of the neutron drip line. This requires the use of liquid tritium targets [62] coming up to 2.5 mm in thickness. The weight of tritium contained in this target will be about 1500 mg, its activity making about 15 Ci. The environment needed for the work with such tritium activity will be created in proximity to the reaction chamber of ACCULINNA-2 where experiments involving the use of tritium targets will be carried out.

Experiments requiring the beams of ^{11}Li, ^{14}Be, ^{24}O are planned for the period 2020–2023. The objective of these experiments will be the study of the ^{13}Li, ^{16}Be, and ^{26}O nuclear systems predicted to be candidates for the true $2n$ emitters [114]. The ^{26}O nucleus draws special attention because of theory [115] imposes stringent limits on its decay energy allowing one to expect that the life time of this nucleus makes no less than 1 ps *i.e.* it exhibits the $2n$ radioactive decay.

Amazing results were provided by the experiments [88–91] where the one-proton knockout from ^{27}F was exploited assuming that the searched ^{26}O ground-state is populated in this reaction. However, a theoretical study [37], made for the population of ^{10}He states in the one-proton knockout from ^{11}Li, showed that strong initial-state effects could be a general drawback for the works using knockout reactions to populate broad states of $2n$ emitting systems beyond the drip lines. This conclusion is relevant in full measure to the case of ^{26}O. Therefore, we face with the fact that the extremely interesting ^{26}O nucleus gives challenge to measure the energy and width of its ground-state resonance. In the second half of the current 7-year period, the U-400M – ACCULINNA-2 tandem will provide conditions (beam intensity, new tritium target) for obtaining precise data on the energy and width of the ground-state and higher-lying resonances of the ^{26}O nucleus. Taking the two-neutron transfer reaction $^3\mathrm{H}(^{24}\mathrm{O}, p)^{26}\mathrm{O}$ one will be able to measure at ACCULINNA-2 the ^{26}O ground-state resonance with energy resolution better than 7 keV. The implementation of the combined mass method will guarantee the achievement of this result in experiments carried out with luminosity making $\sim 2 \times 10^{23}\,\mathrm{cm}^{-1}\,\mathrm{s}^{-1}$.

The noticed upgrade of the DRIBs-3 complex (see the final part of sect. 3 and refs. [65, 66]) is scheduled to be completed in 2021. Looking at the list of RIBs given in table 9, one makes sure that some of the nuclei obtained as fragmentation products of the U-400M primary beams can be extracted and ionized by a conventional ISOL method. First of all, these are helium isotopes ^{6}He and ^{8}He easily obtained from the ECR ion source as a beam of doubly charged ions prepared for injection in the U-400R cyclotron for further acceleration. However, this approach is not effective for many RIB specimens. Therefore, for the full-scale operation of the DRIBs-3 accelerator system a complex involving the gas cell coupled with the RFQ cooler and buncher will be created. The best position for this setup at the ACCULINNA-2 separator is the focal plane F4 where the selected RIBs are cleaned out of the other components of the RIB cocktail.

Recently the strategy of further developments of RIB projects at JINR became the discussion subject. As a result, the international project DERICA (Dubna Electron - Radioactive Ion Collider fAcility) was proposed [116]. It could be unique for the advancement of basic issues in nuclear physics and nuclear astrophysics, including: produc-

tion of still unknown nuclides, their mass measurements, the study of decay modes, fission barriers of heavy nuclei, the study of the nuclear reactions dynamics, and the examination of detailed structure of exotic nuclei, *i.e.* the determination of charge and matter radii made with a record accuracy. The key role in this project is given to electron-nucleus collisions providing information on the charge spatial distribution obtained for the sets of nuclei fitting in the long isobaric and isotopic chains [117, 118]. The conceptual and technical design reports of the DERICA project will be fully completed during the years 2018–2023.

7 Summary

Radioactive ion beams were obtained in 2017 from the new in-flight fragment separator ACCULINNA-2. The design parameters of this facility were experimentally confirmed. The obtained RIB intensities at the final focal plane of the separator, the beam purities and transverse profiles of RIBs hitting the physics target confirm the design parameters. The new ACCULINNA-2 separator will be a basis at the FLNR JINR for research made in the fields of light exotic nuclei near the nucleon stability borders. The first-priority experimental program with RIBs for the new facility is outlined. In particular, ^{7}H, ^{26}O, ^{17}Ne and ^{26}S nuclides and their possible decay schemes proceeding via the $2p$, $2n$ and even $4n$ emission are in the sphere of interest of the ACCULINNA-2 research plans. The setup has a good prospect to be a point of growing to a MEGA science project DERICA with a great discovery potential.

This work was partly supported by the Russian Science Foundation, grant No. 17-12-01367. The authors are grateful to Profs. Yu.Ts. Oganessian, S.N. Dmitriev and M.V. Zhukov for the long-term support and development of this activity. The authors express many thanks to the SIGMAPHI company and to the members of the ACCULINNA team. Also, the authors express their gratitude to the collaborators from other institutions A.A. Korsheninnikov, C. Scheidenberger, O. Tarasov, I. Mukha, O. Kiselev, V. Eremin and E.Yu. Nikolskii for many useful advices and creative discussions facilitating the work on this project.

References

1. T. Kubo, Nucl. Instrum. Methods B **376**, 102 (2016).
2. X. Ma *et al.*, Nucl. Instrum. Methods B **408**, 169 (2017).
3. G. Cuttone *et al.*, Nucl. Instrum. Methods B **261**, 1040 (2007).
4. SPIRAL2, `http://pro.ganil-spiral2.eu/`.
5. ISOLDE, `http://isolde.web.cern.ch/`.
6. ISAC, `http://www.triumf.ca/research-program/research-facilities/isac-facilities`.
7. H. Geissel *et al.*, Nucl. Instrum. Methods B **204**, 71 (2003).
8. M. Winkler *et al.*, Nucl. Instrum. Methods B **266**, 4183 (2008).
9. M. Hausmann *et al.*, Nucl. Instrum. Methods B **317**, 349 (2013).
10. T. Kubo, Nucl. Instrum. Methods B **70**, 309 (1992).
11. T. Kubo, Nucl. Instrum. Methods B **204**, 97 (2003).
12. `http://aculina.jinr.ru/publications.php`.
13. `http://aculina.jinr.ru/acc-2.php`; Letter of intent, The ACCULINNA Collaboration, Version: 10.5 Date: May 20, 2010, `http://aculina.jinr.ru/pdf/app-10-6.pdf`.
14. L.V. Grigorenko, A.S. Fomichev, G.M. Ter-Akopian, Nucl. Phys. News **24**, 22 (2014); `http://aculina.jinr.ru/acc-2.php`.
15. S.A. Krupko *et al.*, EPJ Web of Conferences **66**, 11021 (2014).
16. W. Beeckman *et al.*, in *Proceedings of the 13th International Conference on Heavy Ion Accelerator Technology, HIAT2015, Japan, Sept.7-11, 2015* (JACoW, 2016).
17. Yu.Ts. Oganessian *et al.*, Z. Phys. A **341**, 217 (1992).
18. FLNR, `http://flerovlab.jinr.ru/flnr/u400m.html`.
19. A.M. Rodin *et al.*, Nucl. Instrum. Methods B **204**, 114 (2003).
20. G.M. Ter-Akopian *et al.*, Phys. Lett. B **426**, 251 (1998).
21. S.V. Stepantsov *et al.*, Phys. Lett. B **542**, 35 (2002).
22. Yu.Ts. Oganessian, V.I. Zagrebaev, J.S. Vaagen, Phys. Rev. Lett. **82**, 4996 (1999).
23. R. Wolski *et al.*, Phys. Lett. B **467**, 8 (1999).
24. S.I. Sidorchuk *et al.*, Nucl. Phys. A **840**, 1 (2010).
25. S.I. Sidorchuk *et al.*, Phys. Lett. B **594**, 54 (2004).
26. A.A. Korsheninnikov *et al.*, Phys. Rev. Lett. **87**, 092501 (2001).
27. S.V. Stepantsov *et al.*, Nucl. Phys. A **738**, 436 (2004).
28. M.S. Golovkov *et al.*, Phys. Lett. B **566**, 70 (2003).
29. M.S. Golovkov *et al.*, Phys. Rev. Lett. **93**, 262501 (2004).
30. M.S. Golovkov *et al.*, Phys. Rev. C **72**, 064612 (2005).
31. M.S. Golovkov *et al.*, Phys. Lett. B **588**, 163 (2004).
32. M.S. Golovkov *et al.*, Phys. Rev. C **76**, 021605(R) (2007).
33. M.S. Golovkov *et al.*, Phys. Lett. B **672**, 22 (2009).
34. L.V. Grigorenko *et al.*, Phys. Part. Nucl. Lett. **6**, 118 (2009).
35. A.S. Fomichev *et al.*, Eur. Phys. J. A **42**, 465 (2009).
36. S.I. Sidorchuk *et al.*, Phys. Rev. Lett. **108**, 202502 (2012).
37. P.G. Sharov, I.A. Egorova, L.V. Grigorenko, Phys. Rev. C **90**, 024610 (2014).
38. A.S. Fomichev *et al.*, Phys. Lett. B **708**, 6 (2012).
39. L.V. Grigorenko *et al.*, Phys. Usp. **59**, 321 (2016) (this journal issue is dedicated to the 60th Anniversary of the Joint Institute for Nuclear Research, `http://iopscience.iop.org/issue/1063-7869/59/4`).
40. L.V. Grigorenko *et al.*, Phys. Rev. C **86**, 061602(R) (2012).
41. L.V. Grigorenko, M.V. Zhukov, Phys. Rev. C **91**, 064617 (2015).
42. A.S. Fomichev *et al.*, Int. J. Mod. Phys. E **20**, 1491 (2011).
43. L.V. Grigorenko, M.V. Zhukov, Phys. Rev. C **76**, 014008 (2007).
44. M.J. Chromick *et al.*, Phys. Rev. C **55**, 1676 (1997).

45. M.J. Chromick *et al.*, Phys. Rev. C **66**, 024313 (2002).
46. M.S. Golovkov *et al.*, in *EXON-2014 Proceedings of the International Symposium on Exotic Nuclei* (World Scientific Publishing Co., Singapore 2015) p. 171.
47. P. Sharov *et al.*, Phys. Rev. C **96**, 025807 (2017).
48. K. Miernik *et al.*, Nucl. Instrum. Methods A **581**, 194 (2007).
49. S. Mianovski *et al.*, Acta Phys. Pol. B **41**, 449 (2010).
50. M. Pfutzner *et al.*, Phys. Rev. C **92**, 014316 (2015).
51. EXPERT TDR, `http://www.fair-center.eu/for-users/experiments/nustar/documents/technical-design-reports.html`.
52. V. Eremin *et al.*, J. Instrum. **12**, C03001 (2017).
53. A.A. Bezbakh *et al.*, to be published in Instrum. Exp. Tech.
54. R.S. Slepnev *et al.*, Instrum. Exp. Tech. **55**, 645 (2012).
55. K. Yamada, T. Motobayashi, I. Tanihata, Nucl. Phys. A **746**, 156c (2004).
56. K.L. Brown, D.C. Carey, Ch. Iselin, F. Rotacker, *TRANSPORT*, Report CERN 80-04, Geneva (1980).
57. M. Berz, H.C. Hoffmann, H. Wollnik, Nucl. Instrum. Methods A **258**, 402 (1987).
58. N. Iwasa *et al.*, Nucl. Instrum. Methods B **126**, 284 (1997).
59. D. Bazin *et al.*, Nucl. Instrum. Methods A **666**, 314 (2009).
60. C. Scheidenberger *et al.*, in *EXON-2014 Proceedings of the International Symposium on Exotic Nuclei* (World Scientific Publishing Co., Singapore 2015) p. 491.
61. T. Dickel *et al.*, Nucl. Instrum. Methods A **777**, 172 (2015).
62. A.A. Yukhimchuk *et al.*, Nucl. Instrum. Methods A **513**, 439 (2003).
63. Beam profile monitors, `https://www.ntg.de/en/produkte/teilchen-beschleuniger/strahldiagnose/strahlprofil-monitore/`.
64. S. Lochner *et al.*, *POLAND-Low Current Profile Measurement Readout System*, GSI Scientific Report 2013; *POLAND-Profile Acquisition digitizer*, `https://wiki.gsi.de/cgi-bin/view/EE/POLAND`.
65. G. Gulbekyan, B. Gikal, I. Kalagin, N. Kazarinov, Phys. Part. Nucl. Lett. **7**, 827 (2010).
66. A.G. Popeko, S.N. Dmitriev, G.G. Gulbekian, M.G. Itkis, Yu.Ts. Oganessian, in *Proceedings of the First International African Symposium on Exotic Nuclei, IASEN-2013, Cape Town, South Africa, Dec. 2-6, 2013*, edited by E. Cherepanov, Y. Penionzhkevich, D. Kamanin (World Scientific, 2015) pp. 91–102.
67. Y. Kondo *et al.*, Phys. Lett. B **690**, 245 (2010).
68. Yu. Aksyutina *et al.*, Phys. Rev. C **87**, 064316 (2013).
69. G. Randisi *et al.*, Phys. Rev. C **89**, 034320 (2014).
70. B.R. Marks *et al.*, Phys. Rev. C **92**, 054320 (2015).
71. R. Kalpakchieva *et al.*, Eur. Phys. J. A **7**, 451 (2000).
72. J.-L. Lecouey *et al.*, Phys. Lett. B **672**, 6 (2009).
73. A. Spyrou *et al.*, Phys. Lett. B **683**, 129 (2010).
74. S. Mosby *et al.*, Nucl. Phys. A **909**, 69 (2013).
75. L.V. Grigorenko, M.V. Zhukov, Phys. Rev. C **77**, 034611 (2008).
76. M. Pfutzner, L.V. Grigorenko, M. Karny, K. Riisager, Rev. Mod. Phys. **84**, 567 (2012).
77. M. Pfutzner *et al.*, Eur. Phys. J. A **14**, 279 (2002).
78. J. Giovinazzo *et al.*, Phys. Rev. Lett. **89**, 102501 (2002).
79. H.T. Johansson *et al.*, Nucl. Phys. A **842**, 15 (2010).
80. Z. Kohley *et al.*, Phys. Rev. Lett. **109**, 232501 (2012).
81. A. Matta *et al.*, Phys. Rev. C **92**, 041302(R) (2015).
82. M.D. Jones *et al.*, Phys. Rev. C **91**, 044312 (2015).
83. Yu. Aksyutina *et al.*, Phys. Lett. B **666**, 430 (2008).
84. Z. Kohley *et al.*, Phys. Rev. C **87**, 011304(R) (2013).
85. A. Spyrou *et al.*, Phys. Rev. Lett. **108**, 102501 (2012).
86. M. Thoennessen *et al.*, Acta Phys. Pol. B **44**, 543 (2013).
87. E. Lunderberg *et al.*, Phys. Rev. Lett. **108**, 142503 (2012).
88. C. Caesar *et al.*, Phys. Rev. C **88**, 034313 (2013).
89. Z. Kohley *et al.*, Phys. Rev. Lett. **110**, 152501 (2013).
90. Z. Kohley *et al.*, Phys. Rev. C **91**, 034323 (2015).
91. Y. Kondo *et al.*, Phys. Rev. Lett. **116**, 102503 (2016).
92. K. Ikeda, Nucl. Phys. A **538**, 355c (1992).
93. P.G. Hansen, B. Jonson, Europhys. Lett. **4**, 409 (1987).
94. T. Aumann *et al.*, Phys. Rev. C **59**, 1252 (1999).
95. M. Pomorski *et al.*, Phys. Rev. C **83**, 061303(R) (2011).
96. A.A. Lis *et al.*, Phys. Rev. C **91**, 064309 (2015).
97. L. Janiak *et al.*, Phys. Rev. C **95**, 034315 (2017).
98. Yu.E. Penionzhkevich *et al.*, Eur. Phys. J. A **31**, 185 (2007).
99. A.S. Fomichev *et al.*, Phys. Part. Nucl. Lett. **9**, 806 (2012).
100. T.T. Bohlen *et al.*, Nucl. Data Sheets **120**, 211 (2014).
101. A. Ferrari *et al.*, *FLUKA: a multiparticle transport code*, CERN-2005-10, Geneva, 2005.
102. O.B. Tarasov, D. Bazin, Nucl. Instrum. Methods B **266**, 4657 (2008); LISE++ code, `http://lise.nscl.msu.edu/lise.html`.
103. Yu.E. Penionzhkevich, Yu.G. Sobolev (Editors), *Proceedings of the International Symposium on Exotic Nuclei* (World Scientific Publishing Co., Singapore 2015) `http://exon2014.jinr.ru/`.
104. Yu.E. Penionzhkevich, Yu.G. Sobolev (Editors), *Proceedings of the International Symposium on Exotic Nuclei* (World Scientific Publishing Co., Singapore 2017) `http://exon2016.jinr.ru/`.
105. S.I. Sidorchuk *et al.*, EXON-2014 Proceedings, p. 183.
106. V. Chudoba *et al.*, the same, p. 191.
107. G.M. Ter-Akopian *et al.*, EXON-2016 Proceedings, p. 380.
108. A.A. Korsheninnikov *et al.*, Phys. Rev. Lett. **90**, 082501 (2003).
109. Yu.B. Gurov *et al.*, Phys. Part. Nucl. **40**, 558 (2009).
110. G.M. Ter-Akopian *et al.*, Eur. Phys. J. ST **150**, 61 (2007).
111. E.Yu. Nikolskii *et al.*, Phys. Rev. C **81**, 064606 (2010).
112. M. Caamano *et al.*, Phys. Rev. C **78**, 044001 (2008).
113. J. Gorres, M. Wiescher, F.-K. Thielemann, Phys. Rev. C **51**, 392 (1995).
114. L.V. Grigorenko *et al.*, Phys. Rev. C **84**, 021303(R) (2011).
115. L.V. Grigorenko *et al.*, Phys. Rev. Lett. **1**, 042501 (2013).
116. DERICA project, `http://aculina.jinr.ru/derica.php`.
117. T. Katayama, T. Suda, I. Tanihata, Phys. Scr. **104**, 129 (1992).
118. A.N. Antonov *et al.*, Nucl. Instrum. Methods A **637**, 60 (2011).

Andrey Fomichev is an experimental nuclear physicist. After finishing the Moscow State University in 1986 he was employed at Flerov Laboratory of Nuclear Reactions, JINR. Experiments with radioactive ion beams and related methods were the topic of his PhD thesis in 1996. Since 2005 he is head of the "Structure of light exotic nuclei" department at FLNR, JINR.

Sergey Stepantsov is an experimental nuclear physicist. After graduation from the Moscow Engineering and Physics Institute (MEPhI) in 1978 till now he has been working, nowadays as a senior researcher, in the Flerov Laboratory of Nuclear Reactions, JINR. The area of his interest is designing ion-optical systems for carrying out investigations in nuclear physics with radioactive as well as stable beams. In 1993 he defended his PhD thesis on this theme.

Leonid Grigorenko is a theoretician specialized in the application of few-body methods to the light clusterized nuclear systems. Topic of special interest is two-proton radioactivity and other forms of exotic few-body decays. He obtained a master degree from Moscow Engineering and Physics Institute (Russia) in 1993 and a PhD from Göteborg University (Sweden) in 1998. He worked in the University of Surrey (UK) in 1998-2001 and at GSI (Darmstadt, Germany) in 2002-2003. Since 2004 he has been employed at FLNR, JINR in the group of ACCULINNA fragment separator. He is a corresponding member of the Russian Academy of Sciences.

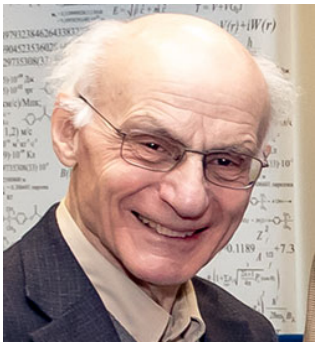

Gurgen Ter-Akopian is a chief researcher in the Flerov Laboratory of Nuclear Reactions, JINR. He carried out experimental studies on several topics: delayed protons, fusion-fission, search for superheavy elements in nature, spontaneous fission, and light exotic nuclei. He made a major contribution in the creation of ion-optical facilities working on the heavy-ion beam lines in the Laboratory: the gas-filled separator BEMS, kinematical separator VASSILISSA, fragment-separator ACCULINNA.

Sergey Krupko is an experimentalist in nuclear physics. He obtained a master degree from Moscow Engineering and Physics Institute (MEPhI) in 2004 and then he was employed at Flerov Laboratory of Nuclear Reactions, JINR. He is an expert in equipment design, detector development and related electronics.